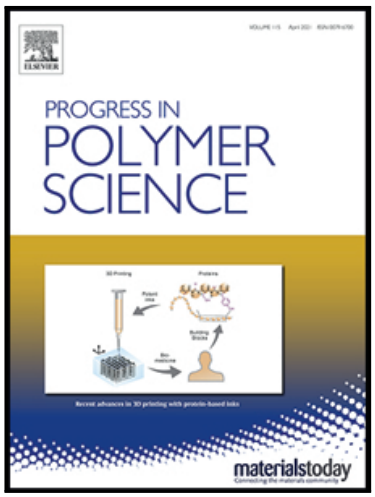

From Pixels to Voxels: A Mechanistic Perspective on Volumetric 3D-Printing

Quinten Thijssen , Joseph Toombs , Chi Chung Li ,
Hayden Taylor , Sandra Van Vlierberghe

PII: S0079-6700(23)00109-0
DOI: https://doi.org/10.1016/j.progpolymsci.2023.101755
Reference: JPPS 101755

To appear in: *Progress in Polymer Science*

Please cite this article as: Quinten Thijssen , Joseph Toombs , Chi Chung Li , Hayden Taylor , Sandra Van Vlierberghe , From Pixels to Voxels: A Mechanistic Perspective on Volumetric 3D-Printing, *Progress in Polymer Science* (2023), doi: https://doi.org/10.1016/j.progpolymsci.2023.101755

From Pixels to Voxels: A Mechanistic Perspective on Volumetric 3D-Printing

Quinten Thijssen†, Joseph Toombs†, Chi Chung Li, Hayden Taylor, Sandra Van Vlierberghe**

† These authors contributed equally.

* Corresponding authors

Q. Thijssen, Prof. Dr. S. Van Vlierberghe

Polymer Chemistry and Biomaterials Group, Centre of Macromolecular Chemistry, Department of Organic and Macromolecular Chemistry, Ghent University, Krijgslaan 281 S4, 9000, Belgium

E-mail: Sandra.VanVlierberghe@ugent.be

J. Toombs, C. C. Li, Prof. Dr. H. Taylor

Department of Mechanical Engineering, University of California, Berkeley, 6159 Etcheverry Hall, Berkeley, CA 94720-1740

Keywords: volumetric 3D-printing, volumetric additive manufacturing, photopolymerization, 3D-printing, volumetric bioprinting

Abstract

The introduction of chemical and/or optical nonlinearity to 3D-printing has paved the way towards volumetric 3D-printing, enabling remarkable advancements in speed, resolution, and the

fabrication of previously inaccessible materials. Given the growing interest of the scientific community, we present a critical review that aims to provide a comprehensive discussion of the potential of volumetric 3D-printing. First, the theoretical framework of photopolymerization is summarized. Subsequent sections highlight the progression of light-based 3D-printing from traditional to emerging volumetric 3D-printing techniques, encompassing both single- and multi-photon polymerization. Special attention is given to the rapidly advancing subfield of volumetric bioprinting which holds great promise for the fabrication of complex multi-material tissue constructs. Finally, critical considerations and limitations of volumetric 3D-printing as well as prospective solutions and opportunities for future research are discussed to allow readers to appreciate and participate in the exciting and rapidly advancing field of volumetric 3D-printing.

Table of contents

List of abbreviations and variables

$[O_2]$	Molar concentration oxygen
[PI]	Molar concentration photo-initiator
μ	Dynamic viscosity
1PA	Single-photon absorption
2PA	Two-photon absorption
2PP	Two-photon polymerization
Ac_{E2}	Excited activator
An_{S1}	Singlet excited-state annihilator

BN	Butyl nitrite
C_{abs}	Absorption cross section
CAL	Computed axial lithography
CLIP	Continuous liquid interface production
C_{sca}	Scattering cross section
CW	Continuous wave
DIW	Direct ink writing
DLP	Digital light processing
DMD	Digital micromirror device
ETU	Energy transfer up-conversion
FITC	Fluorescein isothiocyanate
Gel-MA	Methacrylamide-functionalized gelatin
Gel-NB	Norbornene-functionalized gelatin
hMSCs	Human mesenchymal stem cells
HOMO	Highest occupied molecular orbital
HUVECs	Human umbilical vein endothelial cells
I	Intensity
I_i	Incident irradiance
ISC	Intersystem crossing
I_t	Transmitted irradiance
l	Propagation path length
LUMO	Lowest unoccupied molecular orbital
MA	Methacrylamide
MC	Merocyanine
M_c	Molar mass in between crosslinks
MEMS	Micro-electromechanical systems
MM	Molar mass
N	Number density of particles
NA	Numerical aperture
NB	Norbornene
NIR	Near infrared
o-Cl-HABI	Bis[2-(ochlorophenyl)-4,5-diphenylimidazole]
PCL	Poly(ε-caprolactone)
PDC	Polymer derived ceramics
PEGDA	Poly(ethylene glycol) di-acrylate
PI	Photo-initiator
PIPS	Polymerization-induced phase separation
PVA	Poly(vinyl alcohol)
QY	Quantum yield
r	Distance separating the exchanging participants
RAFT	Reversible-addition fragmentation chain-transfer
S_0	Singlet ground state
Sen_{E1}	Excited sensitizer
Sen_{S1}	Sensitized singlet state
Sen_{T1}	Sensitized triplet state
SF	Silk Fibroin

SLA	Stereolithography
SLM	Spatial light modulator
S_N	Singlet excited state
SP	Spiropyran
SS	Silk sericin
STED	Stimulated emission depletion
SWW	Self-writing waveguides
T_1	Triplet ground state
TED	Tetraethylthiuram disulfide
TEMPO	2,2,6,6-tetramethyl-1-piperidinyloxy
T_N	Triplet excited state
TPO-L	Ethyl phenyl(2,4,6-trimethylbenzoyl)phosphinate
TTA	Triplet-triplet annihilation
UC	Upconversion
UCNPs	Up-conversion nanoparticles
UV	Ultra-violet
VBP	Volumetric bioprinting
VP	Volumetric 3D-printing
α_{ext}	Extinction coefficient
ε	Molar absorption coefficient
λ	Wavelength

1. Introduction

Light-based 3D-printing leverages the synergism between versatile polymer chemistry and the precise manipulation of light. This unique combination provides spatiotemporal control over the polymerization process, and combined with its ability to induce a liquid-to-solid transition, laid the foundation for the field of (light-based) 3D-printing in 1984 [1–3].

This remarkable combination has transformed the way functional 3D objects are fabricated enabling impactful applications in tissue engineering, dentistry, microfluidics, bioprinting, soft robotics, metamaterials and photonics [4–11]. Recent advances in the field of light-based 3D-printing and polymer chemistry have resulted in the emergence of 4D-printing (i.e., 3D objects that are stimuli responsive), post-printing functionalization of 3D-printed objects via Reversible Addition Fragmentation Chain-Transfer (RAFT) polymerization, and the introduction of grayscale 3D-printing [12–16]. Moreover, the emergence of red-shifted photoinitiating systems has paved the way towards 3D-printing of objects in a biologically benign manner [17–19].

Despite the significant advances made, the fabrication of soft objects with intricate geometries at high speeds and without layering artefacts remains a challenge. Novel innovations have addressed this challenge by the introduction of chemical and/or optical nonlinearity to the photopolymerization process, which, when combined with ingenious hardware, enables freeform or volumetric 3D-printing (VP). While the definition of VP is not always unambiguous, it is important to note that in this review, VP is considered as a process that enables freeform conversion of precursor material at an arbitrary position within a volume of material, without requiring secondary operations that relocate precursor material (i.e., absence of relative motion within the material). Building on this definition, VP can be further classified based on the dimensionality of the unit operation. Specifically, volume-at-once printing is a VP process that has the capability to randomly access and polymerize the resin within the entire volume of an object simultaneously.

Several approaches to VP exist to date, employing single- or multi-photon polymerization and leveraging optical and/or chemical nonlinearity to fabricate 3D objects. Current prominent techniques in the realm of VP include computed axial lithography or tomographic VP, 2-photon

polymerization (2PP) and light sheet printing techniques such as xolography. These techniques have revolutionized the field by enabling remarkable advancements in speed, resolution, and the ability to 3D-print previously impossible materials such as solid photoresists. Additionally, VP shows great promise as a tool in the field of bioprinting due to its short residence times, lack of shear forces, and low photoinitiator content.

Given the recent upsurge and increasing interest in the scientific community for VP, a critical review from a mechanistic point of view is crucial to understand the potential of this rapidly evolving field. In this review, we provide a comprehensive examination of the VP techniques available to date, including their mechanisms and applications.

To begin, the theoretical framework for photopolymerization is presented, which serves as the foundation for subsequent discussions. The succeeding section chronicles the application of single-photon polymerization to enable VP and discusses a rapidly evolving tomographic VP technique also known as computed axial lithography (CAL). Subsequently, prospective VP techniques are highlighted that leverage simultaneous and sequential multiphoton polymerization strategies with optical nonlinearity and novel optical parallelization approaches. Moving forward, the considerations and limitations of VP are examined from a polymer chemistry standpoint, accompanied by prospective solutions. Finally, non-traditional approaches to VP are reviewed, followed by future perspectives for the field. Through this comprehensive review, our goal is to provide a thorough understanding of the current and future directions in the exciting and fast-paced progressing field of VP.

2. Photopolymerization in light-based 3D-printing

Traditional approaches in light-based 3D-printing, including stereolithography (SLA) and digital light processing (DLP), leverage (single-photon) photopolymerization in its most basic form, meaning that they do not require supplementary photochemical processes such as (photo)inhibition to locally induce the liquid-to-solid transition to fabricate the 3D object. The aforementioned photopolymerization process refers to a polymerization or crosslinking reaction initiated by photoexcitation, which involves two distinct events: the formation of initiating species and the subsequent polymerization. The purpose of this section is to introduce the fundamental process of photopolymerization in traditional light-based 3D-printing which lays the foundation for subsequent sections. However, readers seeking a detailed discussion of photopolymerization are referred to other sources [13,20–22].

A wide variety of photoinitiators that can be activated by light spanning the deep UV to the visible light region of the electromagnetic spectrum are currently available [17,18,20,23]. When a photon is absorbed, an electron is excited from the singlet ground state to an excited singlet state, with the energy required for this excitation determined by the gap between the Highest Occupied Molecular Orbital (HOMO) and the Lowest Unoccupied Molecular Orbital (LUMO). The spin multiplicity can subsequently change to a triplet excited state (i.e., intersystem crossing (ISC)), and the formation of the initiating species almost unambiguously occurs from the triplet excited state due to its longer lifetime [24,25]. Depending on the type of photoinitiator, the formation of initiating species from the triplet excited state can involve different processes, such as electron transfer, energy transfer, and proton transfer. It should be noted that several processes can compete with radical formation including internal conversion, fluorescence and phosphorescence. Additionally, the excited triplet state can transfer its energy through triplet-

triplet energy transfer or triplet-triplet annihilation. Of particular importance is the ability of molecular oxygen to quench the excited triplet state.

After the initiating species is formed, it triggers polymerization, which comprises three stages: initiation, propagation and termination. During initiation, the initiating species reacts with a monomer to create a propagating species. As the molar mass of the propagating species increases during propagation, it carries the reactive center until polymerization is terminated. Propagation can occur according to three mechanisms: chain-growth (e.g., acrylate polymerization), step-growth (e.g., thiol-ene polymerization) or living (e.g., atom transfer radical polymerization, ATRP, or reversible addition-fragmentation chain transfer polymerization, RAFT). The reactive center responsible for the propagation reaction can be either ionic (anionic or cationic) or radical in nature, and this affects the ability of the photoinitiator to polymerize specific monomers or oligomers. Moreover, the termination reactions involved in ionic- or radical-mediated polymerization differ. Ionic polymerization terminates when a positive and negative charge combine, yielding a neutral molecule that cannot continue propagation. Radical polymerization terminates when radicals combine during recombination, or when an unsaturated bond is formed upon hydrogen transfer during disproportionation. Also here, however, various processes can take place that can terminate the polymerization prematurely of which the most important process is the formation of peroxyl radicals upon reaction with molecular oxygen. Peroxyl radicals are relatively stable and therefore stop the propagation of, among others, (meth)acrylates [26]. Finally, it is important to note the influence of the environment, such as the solvent, on radical recombination (i.e., cage effect), reactivity and stability, as well as chain transfer reactions to the solvent [27].

The previously described light-initiated polymerization or crosslinking process triggers a liquid-to-solid transition, which is exploited to construct the 3D object. Through the deliberate spatial control of the incident light, accomplished using a series of discrete points (as in SLA) or 2D arrays (as in DLP), the solidification of the liquid resin is precisely modulated in space and time, resulting in the desired 3D shape.

3. Volumetric 3D-printing based on single-photon polymerization

The preceding paragraph described the fundamental application of photopolymerization to fabricate 3D objects and, in traditional stereolithographic 3D-printing techniques (i.e., SLA and DLP), the liquid-to-solid transition occurs at the surface of the vat, where it is assumed to receive the highest incident light dose (Figure 1). This results from the fact that the conversion or the extent of single-photon polymerization is directly proportional to the administered light dose, when dose reciprocity is assumed and competing processes such as inhibition are not considered. Consequently, the 3D object needs to be constructed by the gradual accumulation of subsequent outermost layers, with each layer being photopolymerized followed by a resin replenishment step. The resulting layer-by-layer process taking place at the surface of the vat inherently precludes the possibility of VP, reduces printing speed, introduces layering artifacts in the printed objects, and imposes shear stresses during the resin replenishment step.

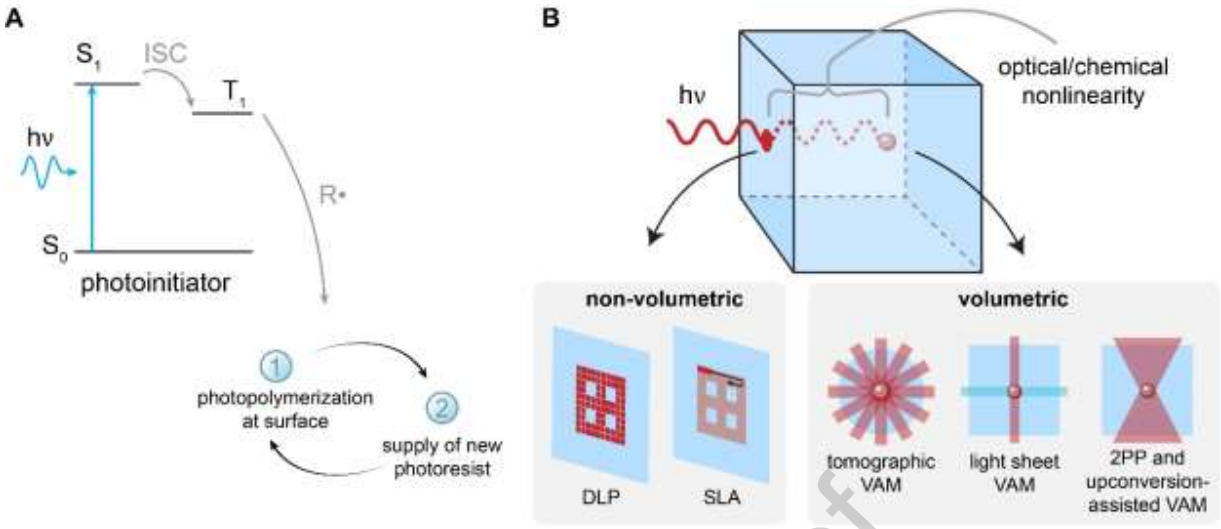

Figure 1. (A) Jablonski scheme illustrating the energy levels and transitions involved in photopolymerization to create the 3D object in a layer-by-layer manner. (B) Schematic depiction of how optical/chemical nonlinearity is able to shift the photopolymerization from the surface of the resin to an arbitrary point within the resin volume and enable volumetric 3D-printing.

3.1 The evolution of single-photon polymerization

The first landmark to move single-photon photopolymerization process away from the surface of the vat was introduced by DeSimone and colleagues through the introduction of a polymerization-inhibited zone. Their approach involved the inhibition of acrylate photopolymerization by allowing molecular oxygen to consistently diffuse into the resin. This zone, which extends several hundreds of micrometers into the resin, remains in a liquid state during the printing process, which enables uncured resin to flow freely beneath the part, eliminating the need for a separate replenishment step. This process is called Continuous Liquid Interface Production (CLIP) [28]. Noteworthy developments in this field include injection CLIP

to overcome speed limitations imposed by passive resin flow, the use of a fluorinated oil to reduce the adhesive forces between the interface and the printed object, and the introduction of photoinhibition via a second wavelength [29–31]. However, while CLIP has eliminated the need for a separate replenishment step, the photopolymerization step remains fixed in its location relative to the resin vat.

Interference lithography is a notable early VP technology that exploits light wavefront modulation or multiple intersecting light beams to create 3D interference patterns which are transferred to a photoresist. While interference lithography is effective for the rapid production of 3D photonic crystals and lattices, the method cannot fabricate arbitrary structures. The 3D light distribution from interfering beams is periodic, hence, the geometry to be printed must be periodic [32,33].The following paradigm-shifting milestone towards VP of aperiodic objects through single-photon polymerization was established by Shusteff and colleagues, who utilized holographically shaped light beams to deliver a 3D light dose distribution to create structures as a 3D unit operation (i.e., volume-at-once VP) [34]. While this approach represents a remarkable departure from 1D or 2D unit operations of traditional 3D-printing, the superposition of a small number of beams limited the versatility of geometries that could be achieved. To address this limitation, Taylor and colleagues introduced tomographic projections as an alternative for the superposition of multiple beams to deliver a 3D distribution of light. This approach, referred to as computed axial lithography or tomographic VP, provided the ability to create fully arbitrary geometries with a 3D unit operation [35,36].

3.2 Tomographic volumetric 3D-printing

As previously mentioned, tomographic VP leverages tomographic projections to deliver a 3D light-dose distribution into a rotating container of photopolymerizable material. Hence, the 3D

object is obtained *volume-at-once* by the superposition of 2D projections that propagate through the transparent resin from numerous directions, in accordance with the principles of reverse computed tomography (Figure 2).

The 3D dose distribution that is administered to the resin induces the liquid-to-solid or solid-soluble to solid-insoluble transition through single-photon polymerization of the resin. Given the fact that the 2D projections propagate the entire resin volume and that only '*in-part'* voxels can be photopolymerized while '*out-of-part'* voxels should remain non-crosslinked, it is crucial that a certain degree of conversion can be obtained without gelation taking place – a conversion threshold is required. In this context, it has been reported that inhibition-mediated non-linearity can be employed to improve the dose contrast between '*in-part*' and '*out-of-part'* voxels. To briefly restate, the local inhibitor concentration must be depleted such that polymerization initiation and propagation (without inhibitor termination) are more probable than radical quenching in order for polymer network growth to proceed. Therefore, the polymer degree of conversion is a nonlinear function of the absorbed light dose which is discussed in more detail in section 5.1 (*vide infra*).

Volume-at-once VP holds significant advantages as it can fabricate 3D parts that have complex geometries, are isotropic and have low surface roughness. Moreover, it is significantly faster than layer-by-layer printing, which builds an object through the sequential addition of 1D or 2D subunits. For instance, printing a 1 cm^3 object using a continuous layer-by-layer process with a layer thickness of 100 μm and an irradiation time of 5 s for each layer would take 8.3 minutes. Conversely, if a hypothetical scenario with identical resin composition and exposure conditions is considered, the volume-at-once VP would only require 5 seconds, equivalent to the time required to add a single subunit. Moreover, the ability of tomographic VP to print into high-

viscosity fluids or even solids eliminates the need for support structures, enables the printing of extremely low-modulus materials, and allows the printing of challenging geometries, including overhanging and disconnected features. Finally, the elimination of layering reduces the surface roughness and anisotropy of the printed part. Finally, tomographic VP has the potential to print around pre-existing 3D structures.[34,36,37]

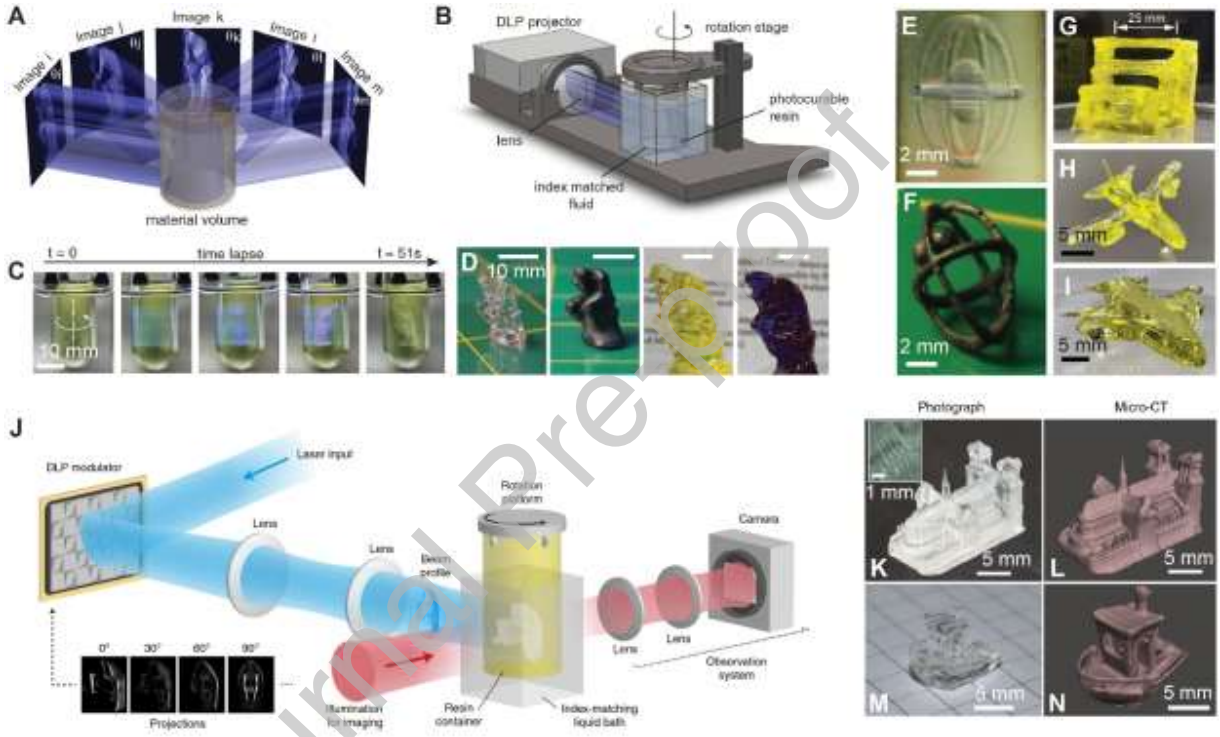

Figure 2. (A) Schematic depiction of tomographic light superposition in tomographic VP. (B) DLP projector-based tomographic VP apparatus. (C) Time lapse of print completed in 51 s. (D) Photographs Thinker models. (E–I) Photographs of polymer objects printed with tomographic VP illustrating support-free printing capability. [36], Copyright 2019. Adapted with permission from American Association for the Advancement of Science. (J) Laser-based tomographic VP apparatus. (K, M) Photographs of polymer Notre Dame and Benchy. (L, N) Micro computed

tomography scans of K and M. [37], Copyright 2020. Adapted with permission from Springer Nature.

As mentioned earlier, acrylate photopolymerization is commonly used in tomographic VP owing to its inhibition by molecular oxygen that introduces chemical nonlinearity to the resin. However, the resulting materials are often glassy and brittle, and their tunability is limited. To address this, thiol-ene photopolymerization has been applied. By manipulating the monomer combination, the modulus and elongation at break of these more uniform molecular networks could be varied over a wide range, while acrylate photopolymerized counterparts showed no such tunability [38]. However, thiols used in thiol-ene chemistry can form thiyl radicals upon reacting with peroxyl radicals that result from inhibition by molecular oxygen, allowing thiol-ene chemistry to proceed in the presence of oxygen. Thus, to achieve the required chemical non-linear dose response, alternative approaches are necessary. An effective approach that has been demonstrated involves the incorporation of 2,2,6,6-tetramethyl-1-piperidinyloxy (TEMPO), which acts as a radical scavenger, into the resin. The inhibitory effect of TEMPO results from the stability of the resulting nitroxide radical that does not participate in further reactions. Section 5.1 discussed the related topic inhibition-mediated nonlinearity in more detail (*vide infra*). Finally, the tunability of thiol-ene photopolymerized materials has been exploited to create temperature-responsive shape memory polymers with variable glass transition temperature ranging from -53 to 55°C [39].

In recent years, there has been a growing interest in the development of multi-material objects with complex 3D geometries using tomographic VP. Multi-material VP can be accomplished in two ways: single-resin versus multi-resin. Single-resin multi-material tomographic VP is

significantly more complex from a resin development perspective as it requires orthogonal photopolymerization to selectively control the solidification of both materials. Furthermore, ensuring compatibility between the involved monomers is crucial, as a homogeneous mixture is essential for achieving the desired multi-material object. Single-resin multi-material tomographic VP was initially demonstrated by employing two photoinitiators sensitive to distinct wavelengths. Visible light was utilized to selectively initiate the free-radical polymerization of acrylates, while UV light was employed to initiate both the free-radical polymerization of acrylates and the cationic photopolymerization of epoxides, leading to the formation of interpenetrated networks (Figure 3A) [40]. This approach enabled precise variation of the material properties throughout the object, making it suitable for applications where varied material properties in a single 3D object are required. Multi-resin tomographic VP, on the other hand, involves the use of multiple resins, which are alternately or simultaneously exposed to create the final multi-material object. To date, multi-resin tomographic VP has been accomplished via three subtly distinct approaches (Figure 3B-3D). Firstly, the object can be printed with additional support pillars that enable the non-crosslinked resin to be exchanged with a second resin, followed by a subsequent photopolymerization step. Secondly, the vial can be filled with two different and separated resins, enabling the simultaneous printing of both materials albeit with a clear division between both in the 3D object. Lastly, a pre-printed construct can be immersed in a second resin, followed by a subsequent photopolymerization step.[41] Multi-resin tomographic VP has been exploited for the fabrication of auxetic meshes consisting of Rhodamine- and FITC-labeled gelatin [41]. However, although both resins were alternately modified, the base material was the same in both cases and consisted of a combination of norbornene- and thiol-functionalized gelatin. Another noteworthy study in this

area used tomographic VP to print multi-material 3D constructs with dynamically tunable perfusion by using a sacrificial template [42]. Both single-resin and multi-resin tomographic VP have advantages and disadvantages, and the choice of approach depends on the specific application and requirements of the final object.

Recently, the capabilities of tomographic VP have been extended beyond the production of polymeric parts through the demonstration of 3D parts made out of glass [43]. This was achieved by combining a technique known as nanocomposite consolidation with tomographic VP, which allowed the creation of 3D parts of silica-based glasses with features as small as 50 µm (Figure 3E). To achieve this, inorganic silica nanoparticles were introduced into an acrylate-based resin. A noteworthy aspect is that positive feature sizes of 20 µm were obtained by introducing TEMPO into the acrylate-based resin in the absence of silica nanoparticles. Finally, an alternative approach to produce inorganic 3D parts is through a technique called polymer-derived ceramics (PDC) through which isotropic, fully dense and crack-free silicon oxycarbide 3D objects were manufactured (Figure 3F) [44].

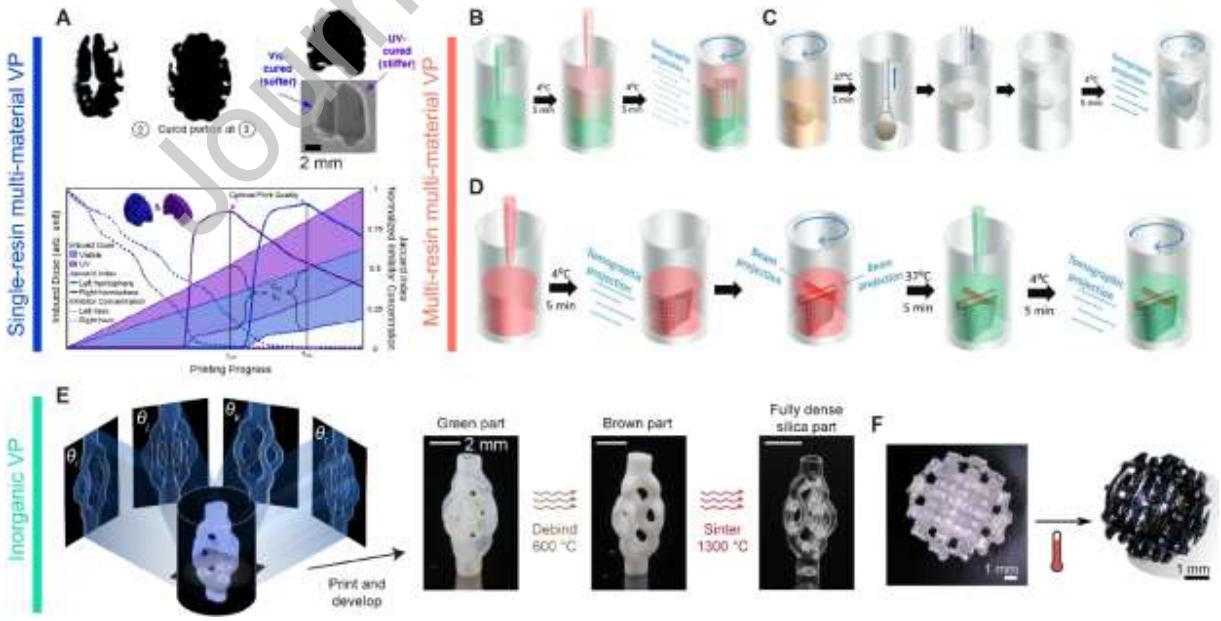

Figure 3. (A) Single-resin multi-material VP. Radical and cationic polymerization are orthogonally triggered to create a 3D brain model with varied stiffness. [40], Copyright 2022. Adapted with permission from Springer Nature. (B-D) Distinct multi-resin multi-material VP strategies. [41], Copyright 2023. Adapted with permission from John Wiley & Sons Inc. (E) Inorganic VP based on nanocomposite consolidation. [43], Copyright 2022. Adapted with permission from American Association for the Advancement of Science (F) Inorganic VP based on polymer-derived ceramic technique. [44], Copyright 2022. Adapted with permission from John Wiley & Sons Inc.

Tomographic VP has also made significant strides in the field of tissue engineering through printing of biodegradable polyesters, achieving positive feature sizes of 100 μm [45]. The resin was based on a thiol-ene photopolymerizable poly(ε-caprolactone) precursor and the printed parts were biocompatible and tunable (Figure 4A). It should be noted that also here, it was shown that the mechanical performance of the thiol-ene photopolymerized materials was significantly improved compared to their acrylate photopolymerized counterparts. Of particular importance is the excellent suitability of tomographic VP for volumetric bioprinting (VBP) due to its short residence times, low photoinitiator concentrations, and absence of shear forces. Tomographic VP was exploited to print liver organoids using methacrylamide-functionalized gelatin (i.e. Gel-MA) (Figure 4C). The bioprinted organoids induced hepatocytic differentiation and albumin secretion, showed liver-specific enzyme activity, and native-like polarization [46]. Iodixanol, a commonly used contrast agent for X-ray imaging, was used to match the refractive index of the resin to that of the organoids. Moreover, tomographic VP was applied to bioprint trabecular bone models with embedded angiogenic sprouts and meniscal grafts, with the latter showing maturation *in vitro* as chondroprogenitor cells synthesized the neo-fibrocartilage matrix [47]. Cell viabilities

exceeding 85% have been reported for Gel-MA-based structures. Another example illustrated the applicability of tomographic VP for bone tissue engineering using a Gel-MA-based resin. High cell viabilities (>90%), and the presence of early osteocyte markers were illustrated in 3D co-cultures of human mesenchymal stem cells (hMSCs) with human umbilical vein endothelial cells (HUVECs) [48]. Moreover, norbornene-functionalized gelatin (Gel-NB) has been processed via tomographic VP in combination with a thiol crosslinker resulting in the rapid formation of 3D parts (< 10 s) with cell viabilities close to 100% (Figure 4D) [49]. It was shown that the stiffness of the 3D hydrogel parts could be effectively controlled over a range of 10–40 kPa by altering the thiol-ene ratio, thiolated crosslinker, polymer content, and degree of substitution. The stiffness of hydrogels is a key factor, which influences the morphology of mesenchymal stem cells (MSCs) and their differentiation [50]. Furthermore, the realm of VBP hydrogels was further extended towards silk-based bioinks [51]. VBP of silk sericin (SS) and silk fibroin (SF) have been reported (Figure 4B). It was illustrated that the former can reversibly shrink and expand, while the latter exhibits tunable stiffness ranging from a few hundred Pa to hundreds of MPa

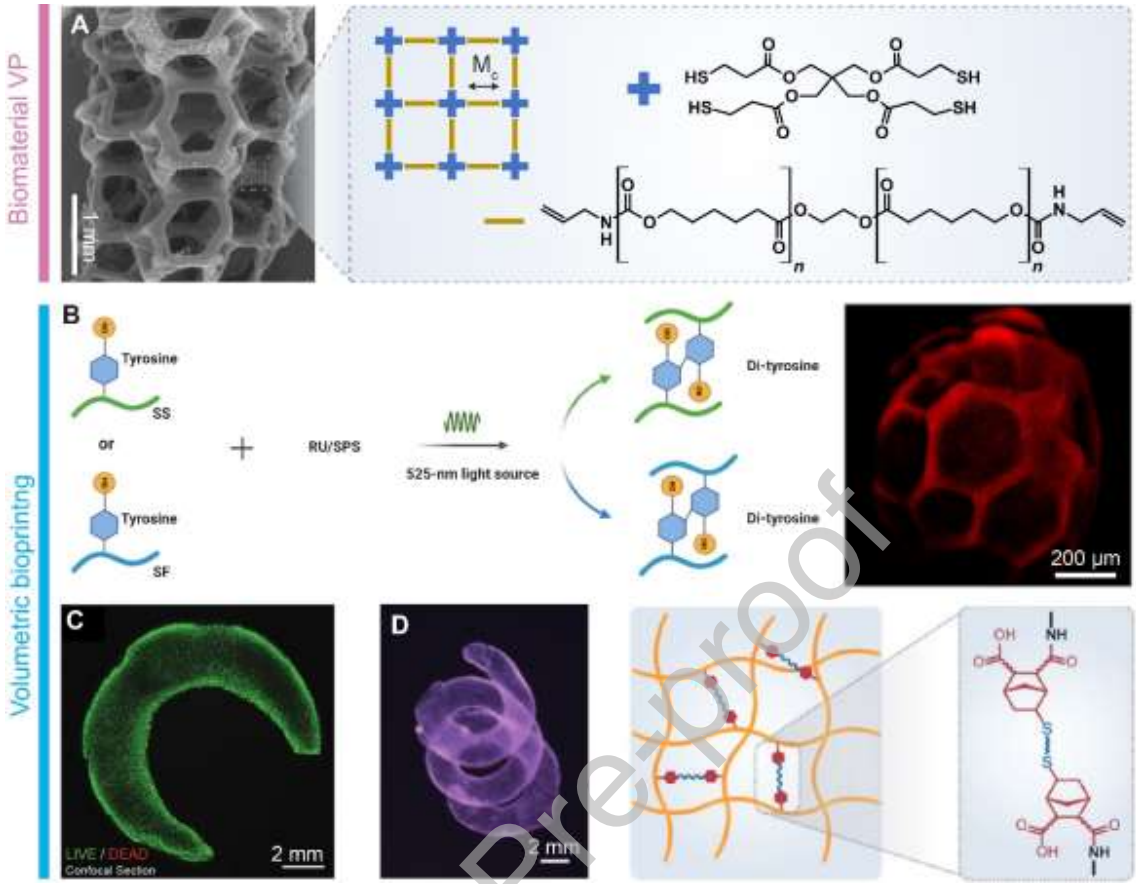

Figure 4. (A) Biomaterial VP of thiol-ene crosslinkable poly(ε-caprolactone) [45], Copyright 2023. Adapted with permission from John Wiley & Sons Inc (B-D) Volumetric bioprinting of: (B) Tyrosine crosslinkable silk [51], Copyright 2023. Adapted with permission from Springer Nature. (C) Methacrylate crosslinkable gelatin [46], Copyright 2019. Adapted with permission from John Wiley & Sons Inc. (D) Thiol-ene crosslinkable gelatin [49], Copyright 2021. Adapted with permission from John Wiley & Sons Inc.

Thiol-norbornene photopolymerization was further exploited to enable fast and efficient VBP of functional ultrasoft hydrogel constructs based on poly(vinyl alcohol) (PVA) [52]. A thermo-sensitive sacrificial gelatin allowed for the creation of stable, stress-relaxing hydrogel constructs

with low polymer concentration that support rapid cell spreading, osteogenic differentiation of stem cells and matrix mineralization. Remarkably, non-reacted norbornene moieties were exploited to immobilize molecules of interest throughout volumetrically printed parts during a subsequent post-polymerization modification (Figure 5A). Tomographic photopatterning is a unique feature of tomographic VP that can be exploited to spatially graft bioactive molecules throughout a previously printed (transparent) material. This approach was later extended to pattern Gel-NB with a fluorescent dye (Figure 5B) [53].. A final application of tomographic VP within the realm of biomedical applications involves the fabrication of three-dimensional printed tablets that are loaded with paracetamol for drug delivery [54].

Recent advancements in the field of VBP have been aimed at expanding the range of materials and the fabrication of multiscale features within a single print to better mimic the complexity of intricate biological structures. To achieve this, the combination of various 3D-printing modalities has been exploited. For example, multiscale organotypic perfusable models with vasculature-like features ranging from 2 to 400 μm were created by post-processing tomographic VP prints through two-photon ablation (Figure 5D) [55]. Another interesting study in this regard illustrated the combination of tomographic VP with melt electrowriting for the creation of multi-material and multi-cellular structures. Noteworthy, melt electrowritten structures were able to provide mechanical support to soft volumetrically printed hydrogels (Figure 5C) [56]. Finally, the combination of extrusion bioprinting and VP has been demonstrated by patterning cells into a microgel-based resin that could be subsequently processed via VP to create multicellular 3D constructs (Figure 5E) [57].

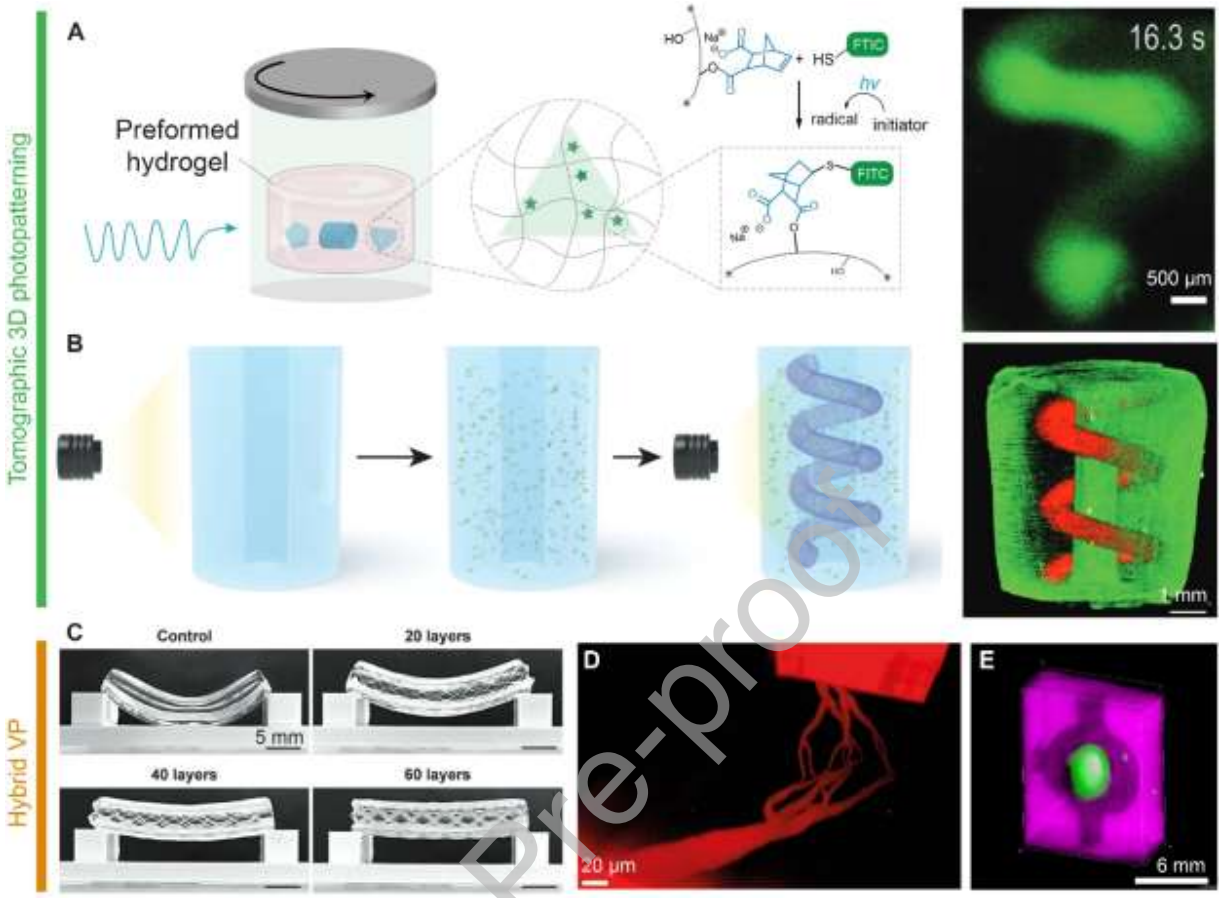

Figure 5. (A-B) Thiol-ene mediated photopatterning of fluorescent moieties in preformed: (A) poly(vinyl alcohol) [52], Copyright 2023. Adapted with permission from John Wiley & Sons Inc. (B) Gelatin 3D constructs [53], Copyright 2023. Adapted with permission from John Wiley & Sons Inc. (C-E) Hybrid VP strategies with: (C) melt-electrowriting [56], Copyright 2023. Adapted with permission from John Wiley & Sons Inc. (D) Two-photon ablation [55], Copyright 2023. Adapted with permission from John Wiley & Sons Inc. (E) Extrusion-based bioprinting [57], Copyright 2023. Adapted with permission from John Wiley & Sons Inc.

In summary, tomographic VP is a promising technology that allows 3D-printing of a wide range of materials, including polymers, ceramics, and cell-laden hydrogels. Tomographic VP is revolutionizing the field of tissue engineering and bioprinting due to its short residence time, low

photoinitiator concentration, and absence of shear forces. As a result, 3D tissue models can be produced with close to 100% viability, outperforming other available bioprinting techniques. Finally, for a more comprehensive exploration of the materials employed in tomographic VP, we refer the reader to a recent review that complements our holistic approach to state-of-the-art volumetric 3D-printing technologies [58].

Several assumptions can be made about the future directions of VBP. Post-printing modification of multi-material and -scale 3D parts is likely to pave the way for constructs that increasingly mimic the intricate complexity of biological tissues, and is expected to be a major driver of future VBP research. Thiol-ene chemistry is considered highly suitable for this purpose, as it allows for easy conjugation of bioactive compounds such as growth factors, cell-binding motives, or antibacterial peptides. Finally, tomographic VP provides unique opportunities in the context of multi-material printing, which is expected to further stimulate research towards mechanically reinforced hydrogels or volumetric printing of tissues with varying degrees of stiffness, such as cartilage.

4. Volumetric 3D-printing techniques based on multi-photon polymerization

Polymerization inhibitors including dissolved oxygen and other persistent radicals induce a chemical nonlinearity in the photopolymerization process which is the fundamental mechanism exploited by tomographic VP. This type of nonlinearity is beneficial because it requires absorption of only a single photon per photoinitiator to operate and can be induced in many different types of photopolymerization mechanisms. However, because the photoinitiating species are generated via linear absorption, spatial selectivity is directly related to the degree of nonlinearity of the polymer conversion vs. absorbed light dose relationship. In this section of the review, we highlight volumetric printing methods which function primarily by optical

nonlinearity, whereby the absorption or production of photoinitiating species is a nonlinear function of the photoexcitation intensity. Given that these methods, in general, require absorption of multiple photons—in some cases, simultaneously or within very short timescales—the required photoexcitation intensity as reported in experimental demonstrations will be emphasized.

4.1 Simultaneous multiphoton polymerization

The emergence of ultrafast pulsed lasers expanded the frontier of 3D-printing by enabling researchers to demonstrate nanoscale volumetric printing via optical nonlinearity—simultaneous multiphoton absorption. The number of photons absorbed per unit time in two photon absorption (2PA) is a function of the field-dependent third-order susceptibility, or hyperpolarizability, of the photoinitiator and has a quadratic dependence on the excitation intensity[59]. Many fields of research including microscopic imaging[60], optogenetics[61], and laser-induced material removal[62], as well as light-based 3D-printing[63] benefit from the spatial selectivity that this nonlinearity provides. Two-photon polymerization (2PP) is commonly used to fabricate micro-optical components[64], scaffolds for cell culture[65,66], as well as optical[67,68] and mechanical metamaterials[69]. While three-photon (or more) polymerization has also been demonstrated, print resolution enhancement that might be expected with a higher degree of nonlinearity is not guaranteed because the wavelength is increased and consequently the diffraction-limited spot size also increases[70]. As industrial appetite grows for nanoscale 3D-printing, so does the need for larger overall build size and faster production speed for mass manufacturing. Along these lines, two thrusts are at the forefront of 2PP research: the development of advanced optical parallelization techniques and the optimization of photoinitiators for higher sensitivity photoresists.

Much effort has been devoted to optical engineering to achieve high scanning speed and/or massively parallelized fabrication[71]. Galvanometer mirrors, whether random-access[72] or resonant-scanning[73], rotating polygonal mirrors[74], MEMS mirrors, and acousto-optic modulators[75] are straightforward tools to enhance volumetric printing rate by rapidly scanning the laser focus instead of scanning the substrate with motorized stages. Generating multiple laser foci with static optical elements including micro-lens arrays[76,77] and diffractive optical elements[72,78] can greatly improve the fabrication speed of periodic structures, e.g., mechanical metamaterials[69] and lattices for cell culturing[79,80], by enabling construction of unit cells in parallel. Furthermore, dynamic spatial light modulators which modulate wavefront phase or impart an amplitude mask have enabled even more advanced configurations. By controlling the phase, multiple laser foci (>1000 in some cases) can be guided independently to create aperiodic structures[81,82] or 3D holograms can be formed to print in volume-at-once mode (Figure 6A–D)[83,84]. Continuous layer-by-layer nano-printing with many similarities to macroscale DLP and CLIP counterparts has recently been achieved using digital micromirror devices (DMDs) combined with spatiotemporal focusing to improve axial resolution[85,86] (Figure 6E–H).

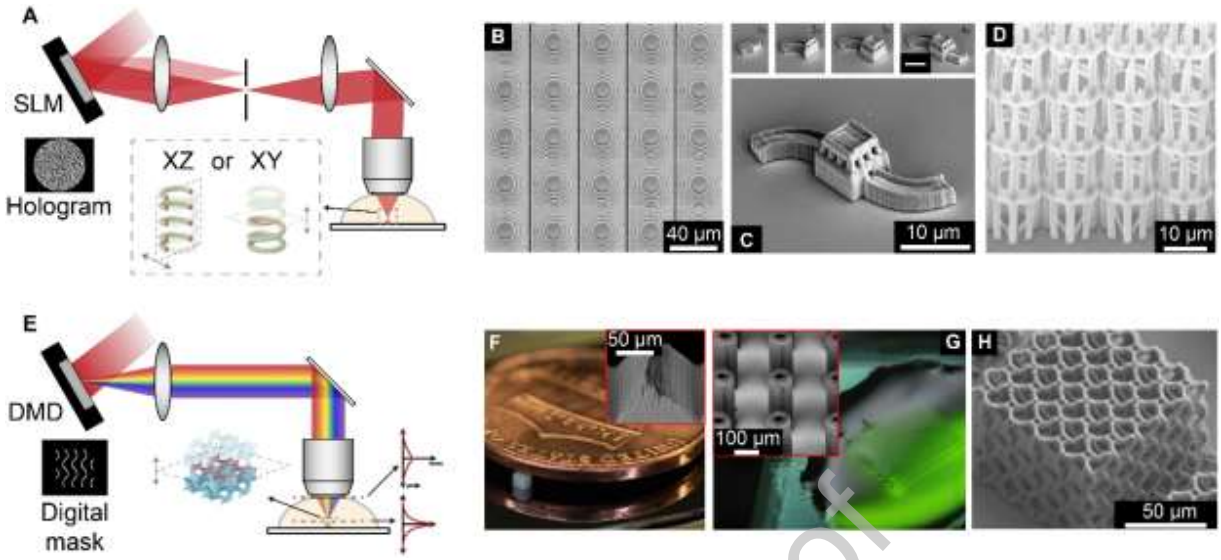

Figure 6. Parallelized 2PP (A) Holographic 2PP enables versatile volumetric nanoprinting in layer-scanning or volume-at-once modes. (B) Fresnel microlens array in holographic layer-scanning mode. [87], Copyright 2020. Adapted with permission from MDPI. (C) Great Wall model in holographic layer-scanning mode. [84], Copyright 2019. Adapted with permission from John Wiley & Sons Inc. (D) 3D microcage array printed in holographic layer-scanning mode. [88], Copyright 2019. Adapted with permission from John Wiley & Sons Inc. (E) Spatial and temporally focused projection 2PP enables DLP-like volumetric nanoprinting. (F, G) Lattice and micropillar array printed with spatial and temporally focused 2PP. [85], Copyright 2019. Adapted with permission from American Association for Advancement of Science. (H) Metamaterial lattice printed with spatial and temporally focused 2PP. Reprinted with permission from [86], Copyright 2021. Adapted with permission from Springer Nature.

Inevitably, multiple foci and higher scanning speed require higher power because the photon flux is either divided amongst multiple voxels or delivered for a shorter period of time per voxel. Given that some methods are already near the boundaries of currently achievable average power, the potential of these high throughput strategies is inextricably linked to the photoresist

sensitivity. Alongside the proposal of these strategies, significant research towards optimization of the photoinitiator has also been underway[59,63,89,90]. Advancements have come primarily from chromophore engineering to increase the 2PA cross-section and, besides the photoinitiator molecule, and from a more developed understanding of the complex efficiency dependence on the environment, e.g., solvent and monomer. A common and successful approach is to maximize the third order hyperpolarizability of the photoinitiator by increasing charge separation. Commonly starting from an effective single-photon photoinitiator, this is done by increasing the π-conjugation thereof through substituting groups with moieties with strong electron donor or acceptor characteristics[91–93]. Increased branching has also proven to increase 2PA cross-section[94]. Reduction of radiative decay, i.e., fluorescence, and, consequently, improvement in the ISC efficiency to the triplet excited state from which the radical is generated, has also been an effective strategy to optimize the overall sensitivity. Comprehensive analysis of monomer, solvent, and photoinitiator properties has revealed that the fluorescence quantum yield is not only affected by the molecular structure but is also dependent on the polarity and viscosity of the photoinitiator's local surroundings[94,95]. It is important to weigh the benefits gained by increasing 2PA cross-section with potential overall sensitivity setbacks that could be associated with decreased solubility or decreased radical generation efficiency. Alternatively, selection of the excitation wavelength near-1PA resonance can also greatly enhance the effective 2PA cross-section[96].

Apart from organic photoinitiators, a newer class of materials, being inorganic metallic nanoclusters, has been found to exhibit large 2PA cross-sections[97,98]. Due to their small size (~1–5 nm) and small number of atoms, nanoclusters possess molecule-like electronic structures. Some 2PA measurements have reported nanoclusters with 10–1000× larger 2PA cross-sections

than engineered organic photoinitiators[99], though there is some debate regarding the accuracy of reported values as 2PA cross-section is difficult to measure with conventional two-photon excited fluorescence methods due to the very low fluorescence quantum yield[100,101]. Nonetheless, recent work has proven the effectiveness of metallic nanoclusters for 2PP printing sub-μm width suspended lines and complex lattices[102]. The nanocluster can also activate a variety of reactions enabling printing of different classes of monomers. The dispersed metallic phase can also lead to enhanced mechanical properties of the printed nanocluster-polymer composite, especially ultimate strength and toughness.

4.2 Sequential or stepwise multi-photon polymerization

To induce 2PA and initiate 2PP, however, high instantaneous light intensity of the femtosecond laser pulse is required. High intensity generally requires tightly focused light and consequently, very small addressable volumes. Though it is generally viewed as an advantage, as evidenced by recent commercial efforts to increase volumetric printing rate by enabling voxel enlargement during printing, an extremely small voxel size is not always required or desirable[103,104]. High peak intensity can induce microexplosion of the photoresist leading to release of gasses and consequently poor print quality. This threshold constitutes an upper limit on volumetric production speed for a given photoresist-optical system combination[89]. On the instrumentation side, special optics may be required to maintain short pulse width for customized systems, e.g., dispersion compensation for micromirror arrays[81,82], and amplifiers may be required to reach the polymerization intensity threshold in each voxel in massively parallelized systems[85,86]. While the cost of ultrafast lasers has been steadily decreasing, the price of a fixed wavelength Ti:sapphire laser, for instance, remains upwards, i.e. $50,000 USD and, with tunable wavelength, > $100,000 USD. Additional expenses arise from the aforementioned specialized optics.

The limited print volume, high peak power, high cost, and relative complexity compared to other light-based 3D-printing techniques can pose a barrier to entry for VP via 2PP. Researchers have sought new photochemical mechanisms to address these deficiencies. Sequential, or stepwise, absorption processes have emerged as a capable alternative for 2PA for nanoscale as well as macroscale printing due their versatility. The key difference between stepwise and simultaneous absorption processes is the existence of an intermediate stage with a lifetime that is not dependent on the pulse duration of the incident light but is governed by slower relaxation mechanisms and often tunable by appropriate synthesis or selection from viable candidates. As we will describe, this transient intermediate stage can take the form of a single or pair of excited molecular electronic state(s) or a reversible isomeric transformation. The volumetric printing technologies reviewed in this section exploit the stepwise nature of the absorption-initiation mechanism to achieve nonlinear effective light dose response at substantially lower intensities and employ novel joint multiwavelength illumination schemes to greatly increase volumetric printing rate. Although research on sequential or stepwise absorption processes for photopolymerization began in the holographic recording field predating direct laser writing by 2PP, the potential this mechanism has to lower the cost, increase accessibility, and realize previously impractical applications of volumetric 3D nanoprinting has become ever clearer in light of the mentioned recent challenges of high throughput 2PP.

4.2.1 Reluctant photoinitiators

α-diketones have a metastable excited triplet state T_1 that has a lifetime within the order of <100 μs and a red-shifted absorption spectrum from the singlet ground state S_0. From this transient state, the molecule can a) be further excited by a photon with wavelength situated in the excited triplet-state absorption spectrum to a higher triplet state $T_1 \rightarrow T_n$—above the bond scission energy

required for photolysis—from which it can initiate free radical polymerization, b) reversibly decay back to ground state, or c) abstract a hydrogen from a donor (or even other α-diketones in the ground state) which is the conventional pathway for Norrish Type II photoinitiation.

An important implication of the red-shifted triplet absorption spectrum is that photopolymerization is nominally confined spatially to the volume of the intersection of two excitation light beams, each with wavelengths situated in the ground and excited triplet-state absorption spectra. When the peaks of these spectra are orthogonal, i.e., well separated with minimal overlap, and two photons of different wavelength are absorbed stepwise to initiate polymerization, the process has been termed *two-color* two-step absorption[105]. Originating in the field of holographic recording, a method was described to "gate" photopolymerization or recording of a hologram with the α-diketone, biacetyl, used as a photoinitiator[106,107]. Biacetyl has a singlet ground state S_0 absorption peak at ~410 nm and triplet ground state T_1 absorption in a wide band ~600–1100 nm. For the hologram, a 752 nm laser was selected, and for optical gating, a UV lamp was selected. When both wavelengths were incident on the photoresist, both transitions—$S_0 \rightarrow S_n$ and $T_1 \rightarrow T_n$—were excited and hologram formation progressed; otherwise photopolymerization ceased. This logical-AND gating effect meant that, after formation, the hologram could be read non-destructively, i.e., without the readout wavelength inducing a photochemical reaction, since only one of the wavelengths is used for readout.

Recently, this approach re-emerged in the field of volumetric 3D laser nanoprinting. Instead of globally gating photopolymerization, a configuration was introduced in which the gating source was focused into a light sheet to activate only a slice of photoresist at an instant in time[105]. By projecting a digital light pattern orthogonally to the light sheet, photopolymerization was initiated where the two beams intersected (Figure 7E and F) Notably, the wavelengths are

reversed in this demonstration because the propagation distance to the focal plane of the projection beam (~500 μm) is larger than the photoresist thickness in the holographic configuration (200 μm). Since the extinction coefficient of T_1 is about 100× larger than S_0 ($\epsilon_{T_1} \approx 100\epsilon_{S_0}$), to achieve sufficient intensity at the focal plane, the blue/UV wavelength which excites $S_0 \rightarrow S_1$ was selected for the projection beam. The intensity threshold for light-sheet printing was determined to be around 10^8–10^9 W m^{-2} for both wavelengths. This is substantially lower compared to the peak intensity of around 10^{15}–10^{16} W m^{-2}[95] required by 2PP which enabled the use of low-cost continuous wave (CW) lasers.

The α-diketone, benzil, has also been used for one-color two-step absorption volumetric 3D laser nanoprinting[108]. Benzil exhibits a special case of two-step absorption in which the red-shifted T_1 absorption spectrum partially overlaps with the S_0 absorption spectrum[109]. For volumetric printing, the excitation wavelength was selected to lie within this overlap such that a single light source—*one color*—could be used to excite both energy-level transitions. Functionally, this operating mode is very similar to conventional 2PP—photopolymerization occurs in the volume where the intensity surpasses a threshold such that the probability of absorbing a second photon $T_1 \rightarrow T_n$ is greater than the probability of decay $T_1 \rightarrow S_0$. Since both photons inherently occupy the same volume because they are focused from one source, the photon flux threshold required for stepwise absorption defines the minimum voxel size. Printing resolution of 100 nm, outperforming stimulated emission depletion (STED) direct write lithography, and in-plane voxel width of 110 nm were obtained. Again, nanoscale printing was achieved with sub-mW laser power provided by an inexpensive CW semiconductor laser diode.

Clearly, an important advantage due to the relatively long metastable triplet state lifetime is that neither excitation light source is required to be pulsed, in contrast to 2PP. Each wavelength can

be supplied by CW lasers or even incoherent sources provided that sufficient photon flux can be achieved. In holography, the UV gating wavelength was supplied by a high-power Hg lamp. Given the impact the use of such low-cost light sources has on the system's expense and complexity, research on stepwise absorption processes for volumetric 3D laser nano-printing and, more generally, volumetric light-based printing is likely to grow rapidly.

To date, screening of other potential photoinitiators which exhibit favorable electronic structures for stepwise absorption has been initiated. Compounds which are modifications of the demonstrated photoinitiators, biacetyl and benzil, as well as other diketones like the well-known cyclic diketone, camphorquinone, were investigated[110]. The study revealed that more than half of the 22 candidate compounds could act as photoinitiators for VP via stepwise absorption with some having increased radical reactivity which further reduced threshold intensity.

For effective two-step absorption, hydrogen abstraction which can occur from T_1 should be limited. Radical quenchers, often stable nitroxide-free radicals like TEMPO, have been used to prevent this side reaction from initiating polymerization which would be, effectively, a single-photon process[105,108]. Alternatively, another approach is to separate entirely the absorption and initiation processes by carefully selecting an absorber which exhibits the two-step absorption behavior (without side reactions) but *does not* induce photopolymerization via primary radical formation and an acceptor to which the absorber's energy is transferred via resonant non-radiative transfer that induces photopolymerization[111].

4.2.2 Photochromic sensitization

While the above-mentioned photochemical reactions have relatively long-lived excited states compared to 2PA, the photon flux required to induce two-step absorption is within the order of

10^8–10^9 W m^{-2}. This intensity is readily achievable with the combination of a high-NA objective and a low power CW laser (<1 mW in some cases). Hence, two-step absorption mechanisms are well suited for geometries with nanoscale critical dimensions. However, large area exposure and consequently, limited NA and lower intensity settings call for a mechanism exhibiting higher sensitivity.

In stepwise absorption, the sensitivity of the light-induced reaction is correlated with the lifetime of the intermediate state. As opposed to an electronic excited state, upon irradiation, photochromic molecules isomerize into a chemical species with a different absorption spectrum. The photogenerated isomer may be thermally stable and the reverse reaction is induced by irradiation in the absorption band of the new species (P-type photochromism) or thermally unstable and the reverse reaction is inevitable and can be accelerated by heating (T-type photochromism)[112]. One prevalent T-type photochromic molecule is the spiropyran photoswitch[113]. The initial spiropyran (SP) compound absorbs primarily in the UV range, and, upon irradiation, a ring-opening transformation produces the isomer merocyanine (MC) form with a new red-shifted absorption peak in the visible range. The MC form has a long lifetime that can lie in the range of 10^{-9}–10^{1} s. Similar to the two-color two-step absorption above, a net nonlinear absorption can occur when the material is irradiated simultaneously by excitation wavelengths in the UV and visible range. (Figure 7B)

The use of photo-switches for photopolymerization, in the context of holographic recording, precedes the use of reluctant photoinitiators (*vide supra*). In 1975, Jeudy and Robillard reported the synthesis of a bi-photochromic compound which enabled nonlinear recording and nondestructive reading[114]. It consisted of a spiropyran conjugated to a benzophenone chromophore. By combining the photo-switch with benzophenone, absorption of a photon in the

MC form which would normally result in reversal to the SP form, yet instead induced hydrogen abstraction by the benzophenone. Along with an electron donor, the reaction produced free radicals and initiated chain-growth polymerization and $\Delta n = 10^{-2}$.

Later, a similar photochromic photoinitiator was synthesized by combining an indole derivative with a nitrobenzyl-containing compound[115]. The nitrobenzospiropyran product had high absorbance <400 nm in the SP form and developed an absorption peak near 580 nm in the MC form. Similarly, polymerization was initiated by absorption of a photon in the MC form and subsequent electron transfer by a co-initiator to the excited MC state. Motivated by elimination of the time-consuming reflow period in top-down SLA, the authors demonstrated that polymerized spikes could be formed at depths up to 3 mm under the surface of the photopolymerizable solution *only* upon simultaneous irradiation at the spatial intersection of orthogonally-propagating UV (324 nm) and red (632 nm) lasers. However, freeform 3D-printing was not reported.

Recently, the photochromic sensitization approach was adopted to demonstrate freeform light-sheet-based VP at the centimeter scale in a process called xolography[116]. Combination of a spiropyran photo-switch with a benzophenone moiety produced a “dual-color photoinitiator”. In the VP configuration, a UV light sheet defined the thickness of a slice of the 3D model while an orthogonally propagating digital light projection defined the in-plane geometry of each slice (i.e., the cross-section). The digital light projection refresh frequency was synchronized with the translation of a container of photoresist such that the object was printed layer-wise within the volume. A variety of geometries were fabricated from complex multibody discontinuous “ball-in-cage” structures to anatomical models which required UV penetration depth up to 30 mm (Figure 7G). Xolography has also been adapted in a continuous flow lithography configuration

where the photoresist was pumped through a flow cell and the light sheet and orthogonal projector fabricated objects within the moving photoresist[117]. The napthopyran photoswitch has also been employed in a similar photochemistry scheme to enable two-color printing[118]. While demonstrations were limited to 2D objects, two-color VP should be possible with the same light-sheet approach used in xolography.

Contrary to the light-sheet printing approach enabled by two-step absorption with an intermediate electronic state, because of the long-lived MC form, the intensity threshold to achieve stepwise absorption with photochromic compounds is relatively low. The aforementioned examples achieved photopolymerization with UV and visible intensity within the order of 10^{-1}–10^{2} mW cm^{-2} [114–116,119]. However, the lifetime of the MC presents a dilemma when analyzing the maximum printing rate. Although the process may be continuous, i.e., without discrete slice-by-slice stepping of the light sheet, consider a scenario in which the light sheet forms a slice of activated photoinitiator and the projected pattern contains a void where polymerization is unwanted. Ideally, the process is time-independent such that, if the next slice contains a "cap" for the void, any light that propagates beyond said slice does not initiate polymerization in the void. In reality, there is necessarily a time dependence related to the rate of back reaction to the SP form. This interlayer parasitic effect is analogous to the so-called cure-through phenomenon in DLP. Thus, the maximum scanning rate of the light sheet is directly dependent on the lifetime of the photogenerated MC form. Because the intensity threshold of stepwise absorption is dependent on the intermediate lifetime, there exists a tradeoff where the sensitivity of the photoresist must be balanced with the desired light sheet scanning rate, and equivalently, the volumetric fabrication speed.

Several investigations reported non-negligible absorbance in the UV range by the MC form or an increase in absorbance in the UV range from SP to MC form[115,116,119]. Since the UV channel is utilized to sensitize the material for subsequent patterning, in the context of VP, this is important to consider because this attenuation directly affects the maximum of at least one of the model's dimensions which is further discussed in section 5.2. Additionally, Regehly and colleagues posit that this absorption could contribute to an initiation channel which competes with the visible absorption channel. In other words, the UV light sheet could contribute to consumption of quenchers or polymerization in regions where this is unwanted, e.g., in the interstices of a sparse lattice.

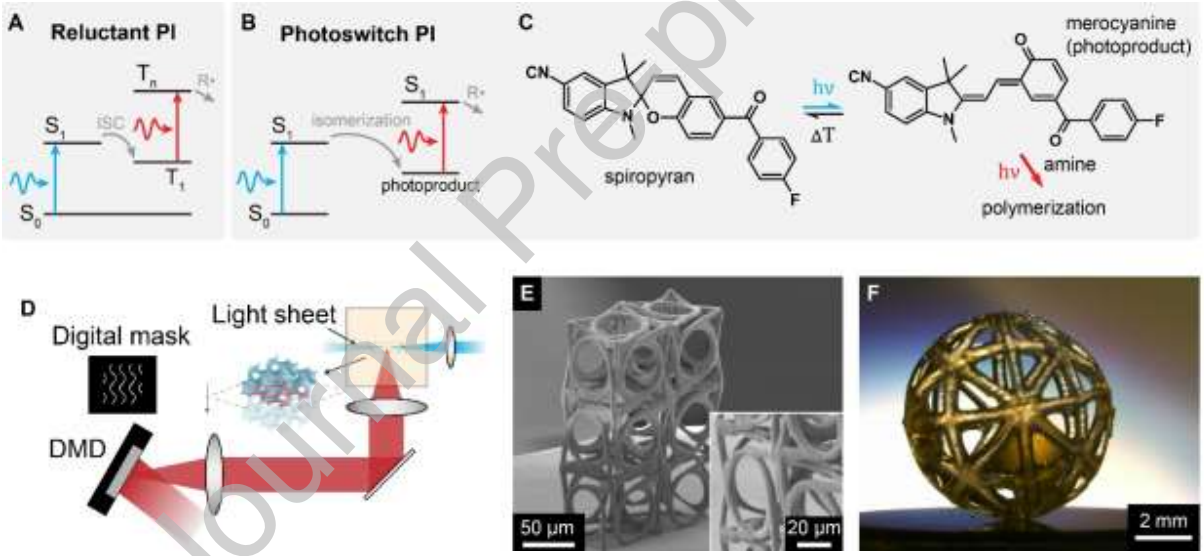

Figure 7. Jablonkski diagrams for: (A) reluctant PI and (B) photoswitch PI or photochromic sensitization. (C) Dual-color photoswitch PI used in xolography: a short wavelength photon induces SP-MC isomerization activating the photoswitch PI. Absorption of a long wavelength photon in the MC form in conjunction with an amine electron donor leads to polymerization initiation. (D) Light-sheet VP is enabled by reluctant and photoswitch PIs. (E) Chiral metamaterial unit cells printed with biacetyl reluctant PI and light-sheet microprinting. [105],

Copyright 2022. Adapted with permission from Springer Nature. (F) Ball-in-cage model printed with photoswitch PI (xolography). [116], Copyright 2020. Adapted with permission from Springer Nature.

4.2.3 Frequency upconversion

Photon upconversion (UC) is a photophysical process which begins with one or more molecules or ions absorbing at least two low energy photons, proceeds through a series of sequential energy level transitions and/or energy transfers, and terminates with anti-Stokes emission of one photon of higher frequency, i.e., higher energy. The long lifetime of metastable excited states (up to milliseconds) makes the UC process different from simultaneous multiphoton absorption and substantially more efficient. Most UC systems discovered result in upconversion of photons in NIR wavelengths to visible or UV wavelengths[120,121]. Operation in the NIR spectrum provides utility in diverse fields of application including biological imaging and deep neuron photostimulation by exploiting the "optical transparency window" in tissue and semiconductor photovoltaics by broadening the usable portion of the spectrum to IR[121,122]. In addition to operation in NIR, the effective nonlinearity of photoluminescence (as a function of excitation intensity) is advantageous for deep volumetric UC-assisted photopolymerization where the emission excites a photoinitiator to initiate local polymerization reaction near the UC emitter[123].

There are many different UC mechanisms and description and delineation of these is beyond the scope of the current review. We direct the reader to other reviews for a more extensive background of the subject[121,124–126]. Here, we focus on two which have been commonly employed in UC-assisted photopolymerization. First, lanthanide ions (Ln^{3+}) have many energy states and they support the energy transfer up-conversion (ETU) process. In ETU, a sensitizer

ion, commonly one with a high absorption cross-section, e.g., Yb^{3+}, absorbs photons and transfers energy to an activator ion, e.g., Er^{3+} or Tm^{3+}. After receiving the energy from two excited sensitizers (Sen_{E1}) sequentially, the activator is excited to the emitting energy level (Ac_{E2}) and emits anti-Stokes photoluminescence upon relaxation to the ground state (Figure 8A).

Second, triplet-triplet annihilation (TTA) has recently gained popularity for UC-assisted photopolymerization in part due to its high efficiency at low excitation intensities compared to other UC mechanisms[127–130]. In TTA, two photons excite two sensitizer molecules, typically transition metal porphyrin complexes, from ground state to the singlet excited state (Sen_{S1}) and the triplet state (Sen_{T1}) after ISC. The energy of two excited triplet-state sensitizers is transferred to two annihilator molecules, typically organic π-conjugated molecules with high fluorescence quantum yield, by intermolecular Dexter triplet-triplet energy transfer. Two triplet-state annihilators collide and undergo TTA resulting in one ground-state annihilator and one singlet excited-state annihilator (An_{S1}) which produces an anti-Stokes emission after ISC and relaxation to the ground state (Figure 8B and C)[131].

The UC photoluminescence intensity is a superlinear function of the excitation intensity where the number of photons required to emit one upconverted photon determines the scaling order. ETU requires at least two excited sensitizer ions to transfer energy to the activator; TTA is a bimolecular reaction between two triplet-state annihilators. In both mechanisms, absorption by the sensitizer is still a linear process. However, since two excited ions or molecules are required for UC, the net photoluminescence effect is nonlinear. Emission occurs only where there is a high population density of excited states such that energy transfer is probable. Non-radiative energy transfer between the sensitizer and activator ions (ETU) and sensitizer and annihilator molecules (TTA) can occur through electrostatic and/or electron exchange interactions. The

probability of these interactions is very sensitive to distance, specifically, electrostatic transfer is proportional to r^{-6}. Electron exchange occurs when wavefunctions overlap and is proportional to e^{-r} where r is the distance separating the exchanging participants[120,125,132]. Therefore, it is crucial that the UC materials are in close proximity, i.e., high concentration, to promote efficient energy transfer.

UC materials are typically deployed in a host matrix or in solution in the form of a nanoparticle or nanocapsule to ensure that their concentration can be high, without requiring large quantities, and flexible to allow for controllable energy transfer efficiency[121,127,129]. The properties and composition of the nanoparticle also have significant influence on the functionality of UC for photopolymerization. Particularly for TTA, UC efficiency in solution is highly sensitive to the presence of molecular oxygen. Due to the electronic structure of molecular oxygen, it can quench the sensitizer triplet state Sen_{T1}, and hence, reduce the probability of energy transfer to the annihilator[122,133]. Depending on its composition, the nanocapsule can provide a barrier to molecular oxygen ingress by diffusion and guarantee higher UC efficiency[134]. Furthermore, a durable nanocapsule shell grown from silica precursor can protect its payload from strong solvents that could be present in photoresists[134]. For both lanthanide-based and TTA UC nanoparticles, surface functionalization of the nanoparticle or nanocapsule can be engineered to enhance solubility and dispersion stability in different polar or non-polar photoresists[122]. The size of the nanoparticle can be designed such that scattering of the excitation light can be sufficiently minimized, and hence, penetration depth maximized[124,134].

Early demonstrations of UC-assisted photopolymerization utilized the long penetration depth of NIR excitation to extend polymerization depth and to perform stereolithographic noninvasive *in-vivo* bioprinting underneath a layer of translucent skin or muscle[123,135–137]. Recently, the

nonlinear photoluminescence has been exploited for nanoscale and macroscale VP with both lanthanide-based and TTA up-conversion nano-particles (UCNPs) [130,138–141]. Direct write lithography was performed at intensities in the order of 10^5 W cm^{-2} in Gel-MA with $NaYF_4$:Yb^{3+},Tm^{3+} UCNPs and in penta-functional acrylate monomer with the biacetyl and 2,5-diphenyloxazole TTA sensitizer-annihilator pair (not combined in delivery nanoparticles)[140,141]. The minimum line width achieved was 1.3 μm in Gel-MA and 50 nm in the acrylate. Other demonstrations have reduced this intensity to the order of 10^1 W cm^{-2} by using TTA UC systems with higher UC photoluminescence efficiency, specifically, palladium metalloporphyrin sensitizers paired with 9,10-diphenylanthracene annihilator[138,139]. The minimum line width achieved was in the range of 0.6–1 μm in acrylate photoresists (Figure 8D and E). Similar UC systems were also used for point-scanning volumetric printing at larger length scales. With $NaYF_4$:Yb^{3+},Tm^{3+} UCNPs, UC-assisted volumetric photopolymerization was merged with standard DLP printing to demonstrate sequential multi-material printing. A palladium metalloporphyrin and 9,10-bis((triisopropylsilyl)ethynyl)anthracene sensitizer-annihilator TTA pair was encapsulated in a robust silica nanocapsule and facilitated both DLP-like and volumetric point-scanning photopolymerization (Figure 8F and G). Furthermore, synthetic modifications of the annihilator enabled tunability of the UC saturation threshold to optimize the UC system for high-intensity point-scanning modes (~10^3 W cm^{-2}) or low-intensity parallel excitation modes (~10^1–10^2 W cm^{-2})[127]. An advantageous characteristic of UC-assisted volumetric printing is the ability to control the voxel size without changing optical components. For instance, simply by increasing the photoinitiator concentration, the penetration depth of light emitted from UCNPs is decreased, and accordingly, the polymerized voxel size is decreased, or vice versa[127,142]. Also, by leveraging the UC photoluminescence saturation

effect, the axial voxel size can be controlled by only changing the excitation intensity[140]. This effect could facilitate adaptive voxel size nanoscale volumetric printing which has been shown to be effective in 2PP. It is important to note that all of these demonstrations utilized either low-power continuous wave lasers or LEDs for photoexcitation.

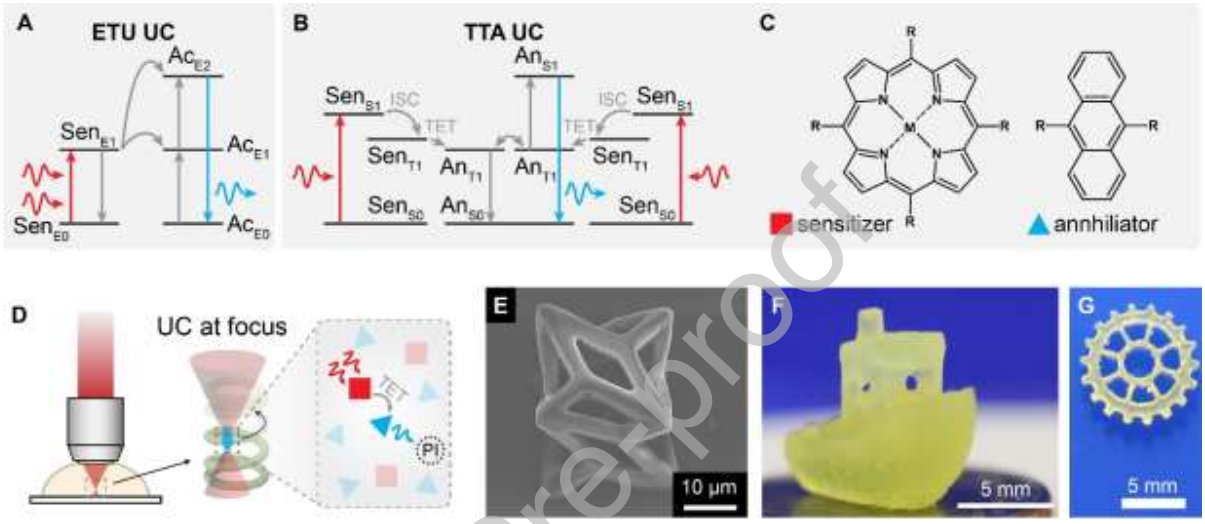

Figure 8. Jablonkski diagrams for: (A) energy transfer upconversion and (B) triplet-triplet annhilation upconversion. (C) Substructures of a common TTA pair: metalloporphyrin and anthracene. (D) UC-assisted VP: two long wavelength photons are upconverted to one short wavelength photon which is absorbed by the photoinitiator. (E) Open strut-like structure printed with point-scanning UC-assisted volumetric nanoprinting. [138], Copyright 2022. Adapted with permission from American Chemical Society. (F, G) Benchy printed with point-scanning UC-assisted VP and gear printed with parallel projection UC-assisted VP. [127], Copyright 2022. Adapted with permission from Springer Nature.

Even though the intensity requirement is already substantially smaller than that of 2PP, UC quantum yield, or efficiency, is still rather low, typically 0.1–10% and up to ~20% for the most efficient TTA UC out of a maximum theoretical efficiency of 50% for two photon

mechanisms[125,126]. However, there are several strategies to increase quantum efficiency which could be impactful for future massively parallelized volumetric printing configurations. Aside from choosing different lanthanides or TTA pairs, indirect methods to improve efficiency of the mechanism can also be considered. Plasmonic resonance can amplify the electric field and indirectly enhance the interaction of the excitation light with the UC materials and enhance energy transfer mechanisms or enhance the emission[143–146]. Methods as simple as incorporating metallic nanoparticles together with the UC materials into a host material have resulted in emission enhancements. With adjustment of nanoparticle size and concentration (to promote proximity to UC materials), enhancements of ~2–5× have been reported[143]. Similarly, metallic nanoparticles may be directly bound to upconverting nanoparticles[146]. More complex multilayer metal-insulator (UC materials)–metal nanostructures designed to maximize plasmon resonance upon absorption of excitation have achieved ~100–1000× UC enhancement depending on the excitation intensity[145]. Alternatively, organic dye molecules anchored to the surface of UCNPs can act like antennae that absorb light and transfer energy through non-radiative Förster-type energy transfer to the UC sensitizer. This strategy greatly enhances UC photoluminescent intensity of lanthanide-based UC providing up to thousands of times higher brightness because lanthanide sensitizers have absorption cross-sections 10^3–10^4 smaller than organic dyes. Organic dye selection is an additional degree of freedom to control the absorption spectrum which is normally confined to spectra of the UC sensitizers with the highest absorption cross-section[121,132].

The most common usage of UC for photopolymerization relies on the photoinitiator absorbing a photon radiatively emitted by the UCNP. There can be substantial inherent losses in the emission-reabsorption process depending on the photoluminescence quantum yield of the UC

emitter and the quantum yield of the photoinitiator. However, similar to dye-sensitized UCNPs, if the photoinitiator molecule is in close proximity (<10 nm) to the UC emitter, it has been demonstrated that energy transfer can also occur through non-radiative modes, like Förster resonant energy transfer, enhancing the overall efficiency of the UC-assisted photoinitiation mechanism[147,148].

5. Considerations related to volumetric 3D-printing

The light-based VP technologies highlighted in this review are transformational for processing materials into 3D objects and they have enabled significant advances in nanoscale fabrication, high-throughput freeform photopolymerization, and bioprinting. With the exciting possibilities and promises of VP, however, there are new challenges and considerations that emerge. In the following section, we have categorized these considerations into logical categories to aid readers who may not be familiar with the field. However, due to the multifaceted nature of VP, there is inevitably some overlap between categories. Whereas 2PP is a relatively well-established technology, it is important to note that we place a stronger emphasis on considerations pertaining to tomographic VP which has seen rapid adoption and research output in recent years. However, we anticipate that many of the challenges and considerations discussed here will also become relevant to sequential multi-photon polymerization VP as it matures.

5.1 Inhibition-mediated nonlinearity

In VP, the resin inherently requires a nonlinear dose response to enable selective photopolymerization of an arbitrary voxel within the resin volume. In early VP, this nonlinearity was achieved through optical means using 2PA[149]**.** However, VP methods such as tomographic VP cannot rely on the aforementioned optical nonlinearity and require an

alternative approach to attain the required nonlinear dose response. This was initially achieved by introducing nonlinearity in a chemical fashion through inhibition of free-radical polymerization of (meth)acrylates by molecular oxygen[150]**.** Upon excitation, the initiating radicals can either initiate propagation or react with dissolved oxygen. Since the rate constant for the reaction with oxygen is typically three to four orders of magnitude higher than propagation, oxygen will first be locally consumed. Hence, it is only after oxygen is depleted that the propagation starts to proceed. This delayed start of propagation is referred to as the inhibition period and allows the resin solidification to occur after at least one cycling period of tomographic light projection (Figure 9A)[44,151]**.**

Several important aspects need to be considered such as the initiator-to-inhibitor ratio, diffusion of initiation and inhibiting species, and light intensity. For robust process control, the resin should be formulated with [PI] > [O_2]. If the initiator-to-inhibitor ratio is close to or below unity, inhibition times are extended many-fold, or even indefinitely, such that polymerization does not take place even despite continuous delivery of light energy[34]**.** Moreover, a feature size dependence exists because of the rediffusion of O_2 into illuminated regions. If the feature size is within the same order of magnitude as the O_2 diffusion length, O_2 rediffuses into the exposed areas, and additional energy is required to cure the respective feature which induces diffusion blurring of the delivered dose distribution[34,37]**.** In this context, the diffusion length is of significant importance, which in turn, strongly depends on the resin's viscosity. Oxygen was reported to diffuse over 100 to 200 μm within several seconds when using low-viscosity poly(ethylene glycol) di-acrylate (PEGDA) resins (μ ~ 0.012 Pa.s), while for a resin based on di-pentaerythritol penta-acrylate with high viscosity (μ ~ 10 Pa.s), the diffusion of oxygen was reported to be less than 2 μm over 20 seconds of printing time. Hence, it was suggested that

printing of detailed structures in low viscosity resins will require operation at reduced oxygen concentration[34,37,152]. A computational model that captures the diffusion of oxygen and feature size dependence of polymerization time that results from said diffusion was experimentally verified and proved that objects with large feature size range that were previously impossible to print became possible by accounting for this effect[152].

While an excess of photoinitiator molecules is preferred for robust process control, the feature size dependence can also be exploited to overcome Abbe's diffraction limit, making the achievable resolution determined by the contrast that is maintained between initiation and inhibition[153]. Indeed, if the laser power is sufficiently low and the initiator-to-inhibitor ratio is close to unity, the photoexcited reaction ultimately stops due to depletion of locally present photoinitiator molecules by in-bound diffusion of oxygen from the surroundings, whereas the refill of initiators is negligible due to their low diffusivity. However, if the laser power is increased beyond a threshold level, polymerization starts to occur locally at the laser focus and operating near this writing threshold has been exploited to write nanoscale solid structures consistently under dynamic inhibition control[151,154]. It should be noted that writing of nanoscale features by diffusion-assisted inhibition imposes certain limitations on the writing speed as it requires that the laser scanning speed allows sufficient time for the quencher to diffuse[154].

Moreover, while the diffusivity of oxygen is governed by the viscosity of the resin, the oxygen concentration is set by the solubility in the respective resin composition, which strongly depends on temperature. Thus, the oxygen concentration is determined by the solubility in the resin at the respective conditions (i.e., temperature). Consequently, the duration of the inhibition period (i.e., the time it takes for the propagation to become dominant over the inhibition) cannot readily be

controlled. Finally, oxygen inhibition in radical initiated thiol-ene reactions is negligible, requiring an alternative approach to induce the inhibition-mediated nonlinearity to the resin. In this context, TEMPO, a potent nitroxide-based radical scavenger, was found to be suitable for creating the nonlinear threshold behavior required for VP[38,43,45]. Interestingly, other stabilizing agents were screened for possible use as inhibitors, but only TEMPO showed the needed threshold behavior[38]. Since oxygen is generally present within the resin as dissolved gas and its concentration is therefore hard to control, it might be favorable to control the inhibition period—even in photoresist compositions which do exhibit oxygen inhibition—with a dissolved radical scavenger such as TEMPO[45]. A potential disadvantage of a dissolved radical scavenger is that it cannot be removed by simply purging the resin with an inert gas, which might limit reusability of the resin. However, reusability of VP resins is an important aspect of future research if the environmental advantages of additive manufacturing are to be fully harnessed.

In addition to inhibitors such as TEMPO and molecular oxygen, photo-inhibitors are of significant interest for VP. Photo-inhibitors differ from other polymerization inhibitors in that the inhibitory effect must be activated by photoexcitation. Prominent examples of photo-inhibitors for free-radical polymerization are o-nitroaromatic compounds[155,156], tetraethylthiuram disulfide (TED)[157–159], bis[2-(ochlorophenyl)-4,5-diphenylimidazole] (o-Cl-HABI)[30,160], and butyl nitrite (BN)[161]. These photo-inhibitors are commonly excited by ultraviolet illumination and the photoexcitation typically produces photo-inhibitor radicals or nitroso compounds that will scavenge photoinitiator radicals or propagating chain radicals to produce inert species. In order to maximize the range of controllable polymerization rates, material systems are typically designed such that the photoinitiation can be independently triggered from the photoinhibition. This can be achieved by carefully selecting photoinitiator and photo-

inhibitor according to their absorption spectra such that one excitation wavelength only effectively excites one of the species but not the other antagonistic species. In practice, this is typically done by using a visible light photoinitiator (such as camphorquinone) that has negligible absorption at near UV wavelengths where a UV-sensitive photo-inhibitor can be excited almost independently. This preferable spectral arrangement is commonly referred to as spectral orthogonality. Moreover, the radical generation quantum yield (QY) of the photo-inhibitor is important as it describes the chance of generating a photo-inhibitor radical per photon absorption event. Photo-inhibitors with high QY (such as o-Cl-HABI with QY close to 2 [162,163]) are preferable as they can produce the same amount of inhibiting species with less photon absorption and allow higher light transmission in VP. In addition, efficient photo-inhibitors require lower excitation light intensity which, in turn, leads to less cross-excitation of photoinitiating species. Moreover, photo-inhibitors such as TED[158,164] and BN[160,161] produce radicals with short lifetimes much less than or on the order of seconds, while other photo-inhibitors such as o-Cl-HABI produce stable radicals lasting from tens of seconds to minutes[30,162,165]. A short lifetime of inhibiting species allows for dynamic modulation of local inhibition strength, and favors applications for direct point-spread function refinement in point-scanning and light-sheet VP modalities. On the other hand, long-lived inhibiting species tend to accumulate, hence, they are naturally suited for encoding 3D volumetric inhibition profiles in volume-at-once modalities such as tomographic VP. Finally, introduction of photo-inhibitors are often accompanied by undesirable side reactions. At concentrations where photoinhibition is effective, photo-inhibitors such as TED undergo significant chain transfer reactions with the propagating chains and slow down polymerization without UV

excitation[30,164]. Formulations with BN showed similar polymerization suppression and this limits acceptable BN concentrations to be well below 3 wt% in methacrylates.[161]

5.2 Light attenuation

In contrast to layer-by-layer printing methods, VP requires the propagation of illumination throughout the entire volume of the resin. In order to effectively address regions deep into the resin, it becomes essential to limit the attenuation or extinction of light (Figure 9B). Extinction refers to the reduction in light intensity as it traverses a medium of absorbing and/or single scattering materials. The extinction coefficient in units of inverse length is given by:

$$\alpha_{ext} = N(C_{abs} + C_{sca}) \quad (1)$$

where N is the number density of particles, C_{abs} and C_{sca} are the absorption and scattering cross sections of the particles[166]. Typically, in the context of VP, the photoinitiator dominates the absorption contribution and has negligible scattering, whereas particulate additives dominate the scattering contribution and have negligible absorption. The absorption contribution is often simplified to be the product of the molar extinction coefficient of the PI, ε, and the molar concentration of the PI, [PI], such that the absorption coefficient can be calculated more easily. The irradiance of a beam of light is attenuated exponentially according to

$$\frac{I_t}{I_i} = \exp(-\alpha_{ext} l) = \exp[-(\varepsilon[PI] + NC_{sca})l] \quad (2)$$

where I represents the incident (I_i) and transmitted (I_t) irradiance and l represents the propagation path length. Note that this formulation assumes the PI is the only species that absorbs light.

To ensure a homogeneous intensity distribution throughout the resin volume, it becomes crucial to control the attenuation of light carefully. This restricts the photoinitiator concentration that can be introduced as excessive photoinitiator concentration would lead to higher absorbance, resulting in increased attenuation and limited penetration depth of the light. Consequently, the curing process would be restricted to a shallow region near the light source, compromising the completeness and quality of the printed object.

Hence, in contrast to the selection of photoinitiators (PIs) for layer-based printing, the choice of PIs for VP requires a combination of low molar absorption coefficient (ε) and high quantum yield at the operating wavelength. This allows for a sufficiently high PI concentration while maintaining a large penetration depth[38]. By carefully optimizing the concentration of photoinitiator, it is possible to strike a balance between efficient absorption for polymerization and minimal attenuation for uniform light propagation. This optimization process involves considering factors such as the desired print resolution, the specific photoinitiator used, the wavelength of light, and the desired cure depth. However, a tradeoff exists between intensity uniformity and print speed. A low concentration of PI minimizes absorption and ensures intensity uniformity of projection throughout the volume but results in longer print times and possibly lower conversions. To compensate for the slower print time, a higher intensity can be used[36]. For tomographic VP, it has been suggested that the illumination time required for curing can be minimized when the resin's absorption coefficient equals the reciprocal of the printing volume's radius, given a specific projector power[36]. Additionally, it should be acknowledged that while inhibitors typically cause negligible attenuation due to their non-absorbing nature (e.g., molecular oxygen) or low concentration (e.g., TEMPO), photo-inhibitor concentrations have been reported to limit the penetration depth as well[160].

Despite the favorable perception of low PI concentrations by the bioprinting community, as they reduce potential toxicity risks associated with high PI concentrations, it can be expected that they will ultimately limit the size of printable objects using VP. Considering the practical example of Gel-MA and the commonly employed Li-TPO-L (ethyl phenyl(2,4,6-trimethylbenzoyl)phosphinate) as photoinitiator, it is possible to derive a quantitative value based on Equation 1. The solubility of oxygen in water, which approximates 0.25 mM, sets the lower threshold for the concentration of the photoinitiator[34]. When taking into account a maximum intensity reduction of 63 % (*vide supra*) across the diameter of the resin container and a molar absorption coefficient of 50 $M^{-1}.cm^{-1}$ at 405 nm, a maximum achievable resin diameter of 35 cm can be determined[36,46]. It is important to acknowledge that this representation disregards the fact that the dissolved oxygen concentration depends on temperature and, can be altered, for example, by purging with an inert gas. To further increase the resin diameter, reducing the molar absorption coefficient and increasing the quantum yield of the PI becomes imperative to ensure sufficient conversion. It should be noted that, alternatively, the inhibitor concentration can be reduced. However, this will ultimately limit the achievable resolution due to loss of the inhibition-mediated nonlinearity. In essence, suitable resins for all VP modalities, especially tomographic VP, should exhibit strong reactivity and low absorption, which differs from the requirements of layer-by-layer printers where both high reactivity and absorption of the resin are necessary to obtain well-defined layers[37].

While minimizing attenuation remains important in VP, there have been proposals to computationally account for attenuation in the projections according to the Beer-Lambert law[37,167]. In initial works related to the superposition of light beams to create an object volume-at-once, transverse intensity profile gradients were applied to the light beams to

compensate for attenuation of other coordinating beams. However, absorption is a nonlinear phenomenon, and beyond a certain point, the spatial nonuniformity of absorbed energy cannot be adequately compensated for by the linear superposition of intensity profiles[34,168]. Similarly to tomographic VP, light-sheet 3D-printing methods require a sufficiently low extinction coefficient at the primary exciting wavelength[105]. Illuminating from several sides or rotating the light sheet of defined intensity distribution around the vessel were proposed to enable deeper printing volumes[116].

5.3 Conversion and post-processing

In layer-by-layer printing, high concentrations of photoinitiators and light doses facilitate near-complete conversion of the green part. However, in VP, there are restrictions on the available photoinitiator and light dosage. Multi-photon techniques are less affected by these restrictions since the respective optical/chemical nonlinearities are not inhibition-mediated. Yet, all VP methods have some need to limit background exposure given their volumetric nature. In tomographic VP, however, the upper limit on the resin's optical attenuation imposes restrictions on the photoinitiator concentration. Additionally, the limited light dose arises from the challenge of delivering a light dose that cures the intended voxels while avoiding unintended curing outside the part boundaries[160]**.** Consequently, the achievable conversion within the part boundaries is restricted in tomographic VP (Figure 9C).

The boundaries of the deliverable light dose are determined by the inhibition period (i.e., inhibitor concentration) and the contrast in dosage between the voxels within and outside the targeted part. An extended inhibition period allows for a higher level of conversion in the in-part voxels, promoting more complete curing of the green part. However, increasing the inhibitor concentration comes at the expense of printing time[45]**.** Furthermore, as previously noted, when

the concentrations of photoinitiator and inhibitor become similar, incomplete crosslinking or cessation of crosslinking may occur.

It is important to note that the low conversions in the green part directly impact its mechanical stability[37,46]. Insufficient curing of the in-part voxels can compromise the overall strength and integrity of the printed object. Consequently, post-processing becomes more challenging in tomographic VP compared to traditional layer-by-layer printing. However, it should be mentioned that tomographic VP also simplifies post-processing of the green bodies due to the absence of a build plate or support structures[44].

Furthermore, the process of photopolymerization plays a significant role in addressing the aforementioned issue. By achieving a sharp change in material properties at the gelation threshold, potential problems associated with a more gradual or linear conversion behavior can be mitigated[169]. The rapid molar mass (MM) increment and concomitant gelation (at 9% conversion if a resin based on small multifunctional acrylates is considered) in case of chain-growth polymerized networks (i.e., acrylates) leads to early rigidification of the network and illustrate a sharp change in material properties. In comparison, the delayed MM increment and concomitant gelation (at 50% conversion if a comparable thiol-ene resin is considered) for step-growth polymerized networks (i.e., thiol-ene) leads to a more gradual evolution of the mechanical properties[170]. This is illustrated by the observation that can be made when comparing the mechanical properties of acrylate photopolymerized materials (chain-growth polymerized network) which are comparatively less affected during post-curing in comparison to their thiol-ene crosslinked counterparts (step-growth polymerized network)[38].

Several approaches have been proposed to address the challenge of developing objects with low conversion following tomographic VP. One straightforward approach is to post-cure the green

part in a solution containing additional photoinitiator. At this stage, the resin outside the intended part boundaries has been removed, eliminating the strict limitations regarding the light dose and photoinitiator concentration. Consequently, the additional photoinitiator can diffuse into the swollen part and increase the conversion upon irradiation. This approach has shown promise in enhancing the mechanical integrity and reducing tackiness of the printed object[45,171].

While ultra-soft structures such as hydrogels are supported during VP, their low mechanical stability during development still poses handling challenges when taken out of the surrounding liquid. Photopolymerized materials require a certain crosslink density (M_c) to withstand gravitational and surface-tension driven collapse. This represents a fundamental challenge when printing porous structures using loosely crosslinked materials. However, a solution has been proposed for loosely crosslinked materials capable of crystallization. By inducing crystallization to the green part while it is still immersed in solution, the mechanical integrity provided by the crystalline domains enables the printing of highly porous designs using loosely crosslinked materials that would otherwise collapse[45].

Finally, an alternative approach for printing soft materials involves a hybrid printing strategy that combines different 3D-printing modalities. Melt-electrowriting, a form of extrusion-based printing, has been employed to build fibrous scaffolds onto which hydrogel structures were printed with tomographic VP. Composite poly(ε-caprolactone) (PCL)-Gel-MA constructs exhibited enhanced mechanical integrity and improved resistance to collapse when removed from developing solution compared to Gel-MA only[56].

An aspect related to conversion that has received little attention in the VP community encompasses polymerization shrinkage stress. In chain-growth polymerization, the most prevalent reaction mechanism in VP, covalent bonds formed between propagating

macromonomers are shorter than the van der Waals distance that separates them (before bond formation) [172,173]. Free volume contraction manifests as shrinkage of the gelling phase. The extent of shrinkage and developed shrinkage stress varies depending on the polymerization mechanism and conversion. A detailed review of shrinkage stress is beyond the scope of this review, but briefly, the delayed gelation conversion associated with step-growth polymerization can result in reduced residual stress build-up compared to chain-growth polymerization [174]. As tomographic VP results in low green body conversion, the shrinkage stress immediately after printing is expected to be low. However, a large fraction of remaining conversion to reach 100% is completed in a post-curing step and shrinkage stress accumulation will happen primarily during this stage. As the field develops, it will be important to investigate how the geometry of the green body coupled with large post-curing conversion affect shrinkage deformation behavior and locations of maximum shrinkage stress. Understanding this effect could lead to software-based distortion pre-compensation schemes to achieve accurate design realization as well as contribute to the design of novel temporal light dose profiles which could incorporate stress relaxation periods. However, ultimately, it is unlikely that shrinkage stress can be entirely avoided by implementing such techniques, hence complementary investigation of low-shrinkage polymer chemistry in VP should be conducted to minimize shrinkage stress altogether. In the upcoming section, a second effect——sedimentation——also caused by volumetric shrinkage and densification from liquid to solid during polymerization is discussed.

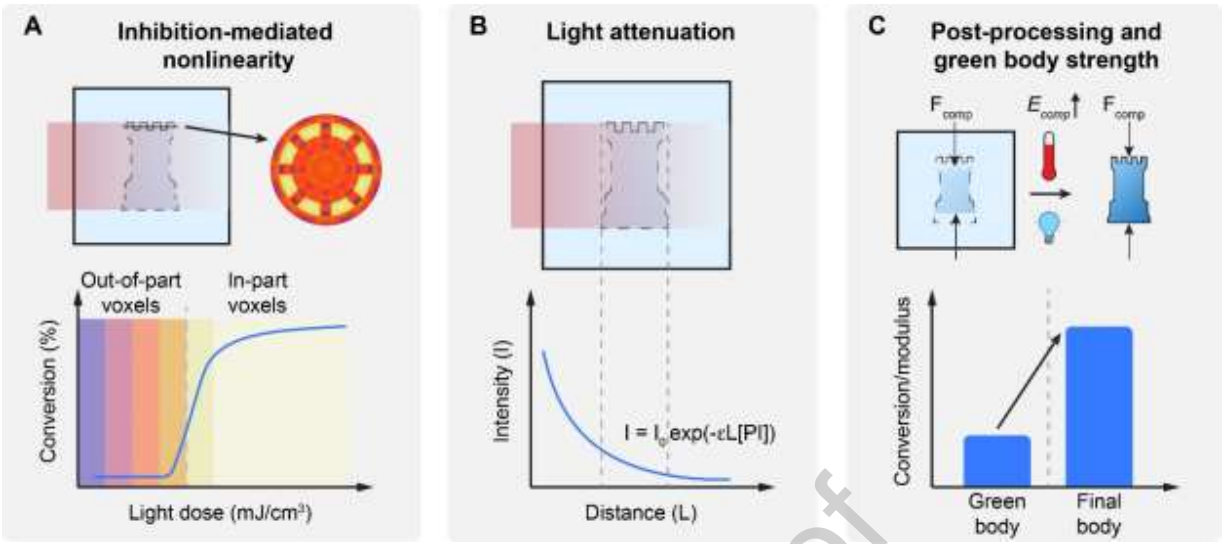

Figure 9. (A) Inhibition-mediated nonlinearity. Nonlinearity is chemically introduced by means of an inhibition period to enable the out-of-part voxels to absorb a certain light dose without noticeable curing, illustrated by the slice of the 3D dose distribution of the printed object. (B) Attenuation of light throughout the print volume according to Beer-Lambert's law illustrating the importance of the photoresist composition in VP. (C) VP requires distinct post-processing considerations to push the conversion in the green body due to the inherently limited light dose that can be delivered during printing.

5.4 Sedimentation

A major advantage that is often claimed for VP is the ability to print with high viscosity and even gel or solid-state materials due to the localized selective photopolymerization provided by chemical or optical nonlinearity. Because there is no relative fluid motion requirement, many geometries can be printed without sacrificial support structures. However, from a different perspective, the necessity that the photoresist must be highly viscous or solid to reduce the detrimental effects of sedimentation can be viewed as a major limitation — not all materials that

would be useful to process with VP are highly viscous and post-printing development is substantially easier with low viscosity materials (Figure 10A).

Although specific thresholds on the required material viscosity to eliminate sinking have been proposed, especially in the context of tomographic VP, the situation is complex and the relative magnitude of sedimentation is dependent on many factors including the monomer chemical structure, the polymerization reaction mechanism and rate, the temperature and exothermic enthalpy of formation, and the spatiotemporal light dose distribution. In this section, we will examine these factors along with several approaches that have been taken to reduce print motion during the printing process and its effects on geometric distortion.

The polymerization chemistry, i.e., the mechanism and monomer characteristics, influences shrinkage and viscosity which are directly responsible for sedimentation. In chain-growth polymerization, after the induction period, there is a rapid increase in degree of conversion and associated high shrinkage as mentioned previously. This nonlinear reaction speed can be beneficial because it means print formation occurs rapidly and, depending on viscosity, the print may be completely defined before any deformation due to sedimentation takes place. On the other hand, in a step-growth reaction, the reaction and increase in degree of polymerization is more gradual, and gelation is delayed compared to chain-growth[38]. Consequently, the period during which deformation due to sedimentation can occur is longer for more linear reactions. Although, in a thiol-ene reaction, for instance, each thiol group reacts with only one ene group which leads to lower shrinkage and sedimentation than (meth)acrylate polymerization where each group may bond with two other monomers[170,175]. Mechanisms like ring-opening polymerization may even result in free volume expansion[173]. In general, regardless of the mechanism, starting with high MM macromolecular monomers (i.e., oligomers) with a low

number of crosslinkable groups leads to low polymerization shrinkage. Although, high MM typically yields high viscosity, which by itself reduces the sedimentation rate. In summary, while freedom of choice of the polymerization mechanism and material composition is not always available, when available, informed design of the photoresist can decrease densification, and therefore, also decrease sedimentation acceleration and terminal velocity.

The viscosity of the photoresist is directly dependent on the temperature. Cooling the photoresist is a simple method to increase viscosity but can reduce the reaction rate. On the other hand, polymerization reactions are exothermic because energy is released in the formation of bonds. This thermal energy generated heats the liquid photoresist surrounding the gelling phase and the gelling phase itself. In particular cases where the heat dissipation is slow and photoresist viscosity is low, convective flows may develop and cause upward motion of the printed part (opposing the gravity vector)[34,176]. This effect is governed by a complex interaction between the polymerization reaction rate, thermal diffusivity of liquid, degree of densification during polymerization, thermal expansion coefficient of liquid and gelling phases, and temperature-dependent viscosity behavior of the photoresist. By describing the process in terms of the two phases, liquid and gelling phase, a simplified model has been used to simulate effects of densification and, separately, heat generation on part motion in tomographic VP[169,177]. To simulate the effects of heat generation together with the polymerization kinetics and shrinkage and validate results experimentally, however, will require extensive material characterization. Nevertheless, undertaking this challenge would be valuable to derive a relationship between the part motion, photoresist material properties, and reaction rate and perhaps would reveal a set of conditions in which sedimentation, buoyancy, and convective flows balance to minimize part motion during printing.

Physical modifications to the photoresist to minimize print motion are commonplace. In VBP, cytocompatible natural and synthetic thermally reversible polymers are typically the backbone of the photoresist. In solution, the long polymer chains interact through physical crosslinking mechanisms like weak hydrogen bonding to form a gel upon cooling prior to printing. Substitution with photopolymerizable functional groups makes the polymers chemically crosslinkable, e.g., Gel-MA, Gel-NB, PVA-MA, PVA-NB, and VP effectively fixes the hydrogel eliminating thermal reversibility with spatial selectivity. This is highly advantageous because sedimentation of printed structures as well as embedded cells is avoided. While these approaches are restricted to aqueous solutions due to solubility, a recent demonstration has proven a similar concept can be extended to nonaqueous organic solutions. In this case, partially ethylated cellulose dissolved in a low viscosity monomer formed a thermally reversible organogel photoresist that enabled overprinting onto embedded structures[178]. Besides physical gelation, incorporation of rigid scaffold structures into the print volume has also recently witnessed growing interest. This intervention may be viewed as somewhat of a regression as supports are often claimed as unnecessary in tomographic VP, but a rigid (in some cases intentionally biodegradable) skeleton reinforces ultrasoft materials, e.g., hydrogels, which may otherwise collapse after removal of excess photoresist[56]. Scaffolds also enable multiple-step printing maintaining dimensional registration between printed subparts during sequential printing and auxiliary operations. So far, these techniques have been demonstrated primarily in the context of tomographic VP but will certainly be important for emerging light-sheet scanning VP techniques, e.g., xolography, multistep absorption and up-conversion-assisted light sheet methods, when the part is not anchored to a substrate.

The viscosity of a liquid is commonly modified by using colloids. An area of research which recently emerged within the VP field is the inclusion of pre-oligomerized or physically gelled microgels. Microgel stacking introduces a small but finite yield stress to the photoresist such that, upon sufficient agitation or shear stress, the colloid assembly flows enabling direct ink writing (DIW) into a VP print container[57]. Due to this shear thinning property, sedimentation of direct ink-written structures and volumetrically printed objects is avoided and excess material flows away easily. Silica nanoparticles were used in UC-assisted point-scanning volumetric printing to increase the viscosity of the monomer for self-supporting structures[127]. Even though they were necessary for tomographic VP of glass, silica nanoparticles included in a nanocomposite photoresist created high zero-shear viscosity which was beneficial to prevent sedimentation during printing and substantial shear thinning behavior which aided in development[43]. Colloidal gels and microgels have been the focus of intensive research in the DIW 3D-printing field and much research could be translated to VP[179].

As effective as physical gelation and viscosity modification may be to minimize print motion, additives may not always be compatible with the photoresist and/or they may not be desirable due the potential to impact negatively, for example, the ultimate conversion and correlated mechanical properties of the product. In these cases, alternative approaches related to modification of the spatiotemporal light dose profile may be considered. The onset of densification and hence, sedimentation, is dependent on the light dose history of each voxel. In tomographic VP, dose optimization algorithms, preferentially weighting high dose uniformity is important to ensure that all voxels proceed through polymerization and densification together, i.e., low differential sedimentation. However, optimization algorithms typically must trade off dose uniformity with dose contrast (between the out-of-part and in-part voxels) meaning that as

the risk of differential sedimentation decreases, the sensitivity of the photopatterning process to optical aberrations and nonidealities increases[180,181]. Alternatively, rebinning the projection intensity history for each voxel to bias high intensity towards the end of exposure has been demonstrated to be an effective way to confine the post-gelation polymerization to a shorter window of time and thus, minimize sedimentation during exposure[181]. In a related approach, a high intensity flood lamp (more than an order of magnitude higher than digital projections) was activated just before gelation—coinciding with the end of the induction period—to complete polymerization rapidly and avoid distortion due to sedimentation in a low viscosity monomer[182].

Understanding the rheological characteristics and dynamics of the photoresist is critically important for successful implementation of unsupported VP. A variety of approaches to minimize sedimentation have been proposed. Nevertheless, sedimentation will continue to be a subject of further investigation as more and more materials are explored, and alternative solutions are required. *In-situ* imaging feedback (discussed in the next section) to track sedimentation and update digital light projections in real time has been proposed as a purely computational approach to the problem[183,184]. Setting aside several challenges including the material optical properties and imaging modality used, in brief, the combination of high temporal resolution and high dimensional accuracy of registration is challenging and is expected to limit the scope of compatible photoresist materials to those with slow reaction rates.

5.5 Optical aberrations

In VP methods, there are multiple sources of optical aberrations: (1) polymerization-induced scattering and refraction, (2) scattering due to dispersed additives with near-wavelength or sub-

wavelength dimensions, and (3) absorption and refraction due to embedded macroscale objects (Figure 10B and C).

Generally, as described in section 5.4, density increases as a result of bond formation and increase in the degree of polymerization. Besides sedimentation, an optical effect of densification is increased refractive index. In practice, subpixel spatial variation in intensity in digital light projection images is inevitable and especially prevalent from laser speckle in partially coherent laser-based systems. Nonuniform intensity seeds the formation of a nonhomogeneous refractive index distribution. Light is focused by regions of higher refractive index which results in faster polymerization and further refractive index heterogeneity, effectively establishing a positive feedback loop that leads to filamentation or self-writing waveguides (SWW)[185]. Microscale self-organization is advantageous for some applications where the pattern of microchannels and microfilaments promotes unidirectional cell migration and alignment for anisotropic tissue engineering[186] and where the ultra-high aspect ratio of the SWW is used to produce hierarchical lattices with characteristic dimensions spanning a large range[187–189]. However, in tomographic VP, the formation of filaments upon gelation—which is typically prior to completion of patterned light exposure (see section 5.3 on green part strength)—can distort the digital light projections and impact the fidelity of printing and roughness of the printed object's surface[182].

Along with densification and refractive index change, the miscibility of a reacting monomer in solution with non-reactive guest solvent (or polymer) changes, which may result in polymerization-induced phase separation (PIPS)[190]. The dynamic competition between the polymerization reaction which restricts molecular mobility and phase separation which drives mixture components apart can be leveraged to create porous microstructures with intensity-

controlled morphology[191,192]. An inherent potential consequence of phase separation is heterogeneous refractive index distribution if the phases have different refractive indices. In cases where the pore size is near or greater than the excitation wavelength, the body is scattering which can distort digital projection images. Similar scattering effects emerge when microscale or near wavelength-sized particles are added to the photoresist. Composite photoresists with a liquid monomer binder phase and solid dispersed particle phase are especially important in 3D-printing because they enable low-shrinkage VP of materials like glasses and ceramics which, historically, have been challenging to process due to brittleness and high melting temperatures.

On the other end of the relevant length-scale spectrum are macroscale aberrations which include large objects (relative to the excitation wavelength) embedded within the photoresist prior to printing or the printed object itself. Clearly, opaque embedded objects will occlude directed or digitally patterned photoexcitation and prevent the formation of particular geometries, while aberrations caused by transparent embedded objects or the polymerizing body itself could be tolerated provided that they would not distort photoexcitation beyond recovery by computational pre-compensation. This concept is described in the next section.

5.5.1 Mitigation of optical aberrations

A physical strategy to mitigate scattering effects of additives is to tune the composition of the liquid phase with reactive or non-reactive components such that the refractive index of the mixture is near that of the dispersed phase. The extent to which refractive index tuning is required to mitigate scattering depends on the wavelength of light and size of scatterers according to scattering theory[193]. This strategy has been particularly effective in 2PP and tomographic VP for composite photoresists containing glasses with low refractive index like silica through the use of monomers with similar refractive index[43,194,195] and for aqueous

biological inks containing cells or multicellular organoids through the use of a liquid, iodixanol, commonly used to “clear” biological samples for microscopy[47,55]. Polymerization-induced scattering can be mostly avoided in scanning-based volumetric methods by appropriate design of the beam focus path or light sheet scanning direction with respect to the printed geometry. However, volume-at-once methods are more susceptible to these effects because all voxels are illuminated simultaneously and for a short duration after gelation. Depending on the magnitude of the refractive index change at gelation, this scattering can be detrimental to the microstructure and surface morphology. In this context, iodixanol has also been employed to increase the baseline refractive index and decrease the nonlinearity to eliminate filamentation at concentrations up to 50% w/v[55]. At high concentrations of iodixanol (10–50% w/v), the gelation behavior was not affected; however, the shear and compression moduli were significantly decreased because crosslinking density was lower[47,55]. For all types of photoresist formulations where scattering by particles is problematic, including aqueous and organic, the mechanical properties vs optical transmission tradeoff is expected to be present when a non-reactive component is used to control the refractive index of the matrix phase.

Computational methods offer strategies to compensate for optical aberrations without modification of the photoresist. Attenuation by embedded or previously printed objects is relatively straightforward to simulate and compensate for when excitation comes from only one or a few directions as in 2PP and light sheet scanning VP. However, when photoexcitation comes from many directions in tomographic VP, the limitations on printable geometry imposed by the shape of the embedded occlusion are not as clear. According to the Fourier slice theorem, assuming negligible material attenuation, angular coverage >180° is sufficient to reconstruct perfectly an arbitrary geometry in a tomographic reconstruction. This implies limitations when

the embedded object is nonconvex, because, by definition, concavities restrict accessibility to <180°. The result of restricted accessibility (similar to the “limited angle” problem in computed tomography[196]), however, depends on the spatial frequency content of the geometry to be printed. For example, for a specific lattice-type geometry, substantial degradation in reconstruction quality was only observed <120° angular coverage[197].

There has been limited analysis of geometric feasibility and angular accessibility topic in the context of embedded objects with treatments ranging from neglecting light occlusion for simple axisymmetric embedded objects[36] to empirical measurement of attenuation in order to identify embedded geometries which have minimal influence on printing such that occlusion can be neglected[56] to modeling occlusion in the light propagation model of the dose reconstruction.[178] Transparent embedded objects are yet to be considered. However, analytical rebinning and geometric ray tracing approaches have been developed to accommodate light refraction by the photoresist and container in non-ideal tomographic VP configurations[198,199]. Especially in systems without telecentric optics, these approaches have demonstrated the ability to maintain high print fidelity without the constraint of maximum build volume size being less than the size of the optics.

Scattering aberrations are most apparent in centimeter-scale VP where attenuation by large concentrations of additive particles significantly decreases the light penetration depth. Due to the nonuniform angular spreading of light as described by the scattering phase function, scattering also attenuates high spatial frequencies in digital light projections faster than low spatial frequencies –the material acts as a low pass filter with decreasing cutoff frequency for increasing propagation length[167,193,200]. Rather than full simulation of a scattering light propagation model, one heuristic approach to counteract this affect is to apply a propagation length dependent

high pass filter on the target model such that the relative magnitude of spatial frequencies is balanced. *In-situ* empirical measurement of the spatial frequency attenuation provides a simple means to gather the necessary correction mask. With compensation, the resolution and fidelity of tomographic VP could be improved in photoresists with concentrations of cells up to four times higher than reported in the state-of-the-art and for low concentrations of TiO_2[167]. With optical changes in the apparatus (see section 6) such as increased wavelength to take advantage of the scattering dependence on λ^{-4} in the Rayleigh regime, for example, or using a coherent source and phase modulation, we expect the maximum tolerable scattering to increase even further.

We have discussed these physical, optical, and computational mitigation strategies separately, but in practice, we envision that a combination of approaches would be used to achieve the best results when optical aberrations are problematic.

5.5.2 Metrology

Taking advantage of polymerization-induced changes in the optical properties of the photoresist, several *in-situ* inspection techniques have been developed for VP techniques. As the refractive index of the photoresist typically increases with crosslinking density, spatially varying and time-dependent changes in refractive index result in varying phase shifts which can be observed directly with coherent and incoherent phase imaging strategies. In 2PP, several strategies have been implemented to inspect the formation of microstructures. Optical coherence tomography was used to reconstruct 3D microstructures with dimensional resolution of about 3 μm and nominal refractive index sensitivity of 3.8×10^{-4} [201]. Optical diffraction tomography achieved diffraction-limited dimensional resolution of 200 nm and 500 nm in the lateral and axial directions, respectively, with imaging exposure time of 6 ms [202]. A non-interferometric method based on phase retrieval from intensity images by the transport-of-intensity equation

with structure height resolution better than 1 μm was developed[203]. In tomographic VP, an incoherent method called color schlieren tomography was used to reconstruct the evolving 3D refractive index distribution during a print with refractive index sensitivity on the order of 1×10^{-4} and to observe dark polymerization effects after illumination ceased[183,204]. Scattering generated by polymerization-induced filamentation/SWW and phase separation can be observed as an attenuation in bright-field imaging modes or the signal itself in dark-field imaging modes. By illuminating the photoresist coaxially with rotation axis and imaging perpendicularly to the rotation axis in tomographic VP, side-scattered light was observed after gelation and azimuthal projections of the scattered light intensity were used to reconstruct the printed 3D object through a technique called optical scattering tomography[184]. Not every material of interest in VP exhibits easily detectable refractive index changes or scattering, such as compositions with a large fraction of non-reactive diluent[205]. Hence, a universal *in-situ* metrology technique is elusive; increasing the sensitivity of the imaging modality usually results in a smaller signal range which narrows the scope of applicability to different material systems.

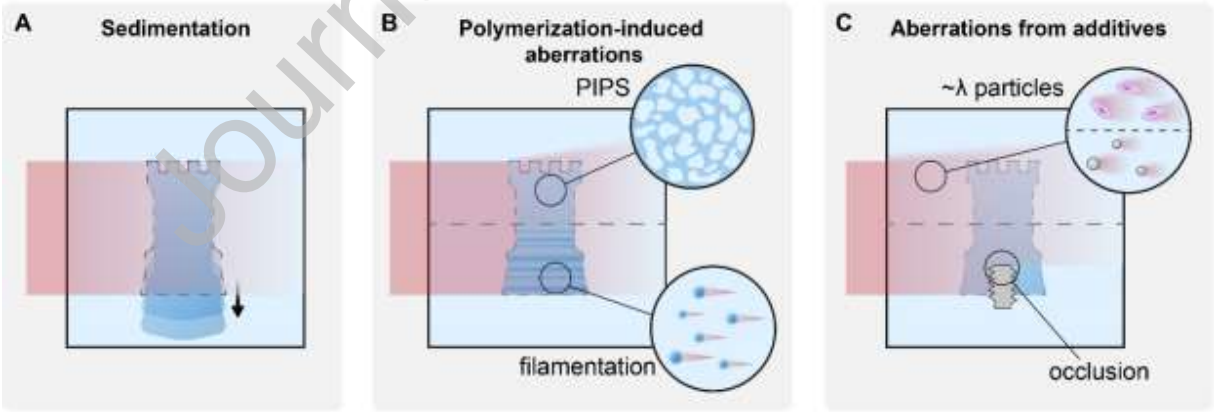

Figure 10. (A) Sedimentation occurs when the polymerizing body densifies and a liquid photoresist is used. If sedimentation begins prior to completion of the light exposure, blurring effects can impact the print quality. (B) Polymerization-induced aberrations including PIPS and

filamentation scatter light and impact print quality primarily after polymerization has begun. (C) Aberrations from additives including near wavelength-scale particles like cells or inorganic nanoparticles or macroscale embedded occlusions scatter or occlude exposure light.

6. Non-conventional volumetric 3D-printing

It is clear that, for certain material systems, the requirement of precursor transparency for VP is challenging — in extreme cases impossible — to achieve through precursor composition tuning or computational methods at the near-UV and UV wavelengths commonly used. Within the realm of light-based methods, significant advances have been enabled by red-shifting the illumination into long visible and near-IR wavelengths. 2PP and up-conversion-assisted VP, as mentioned previously, commonly utilize NIR wavelengths and are inherently well suited for highly scattering materials. Though most demonstrations of tomographic VP to date have used wavelengths in the range 350–550 nm, we anticipate increasing interest in longer-wavelength illumination to enable further material processing innovations, especially for scattering composite photoresists and biological inks with high concentrations of embedded cells that have particularly acute phototoxicity to UV or near-UV light[206–208]. Indeed, focused microwave energy has been proposed to expand the range of materials and, early proof-of-concept experiments showed that time-reversal wave propagation algorithms enable energy localization (by a microwave antenna phased array) sufficient to cure an opaque epoxy resin[209]. Similarly, long coherence length photoexcitation and wavefront shaping, which have been used extensively for deep photo-stimulation in highly scattering biological tissues, could be readily adopted for photopolymerization of challenging composite materials as a form of phase-modulated VP[210].

Besides electromagnetic energy, sound — which propagates through a material as variations in pressure in a compressible medium — is transmitted through many materials opaque to UV-NIR

light. Ultrasound energy typically in the frequency range of 10 kHz–1 MHz focused to a point can induce cavitation in liquid materials and, consequently, rapid heating and cooling where the pressure amplitude is sufficient. Heating can induce polymerization by self-initiation or thermal free radical initiators. Due to the rapid cavitation heating-cooling cycle and corresponding spatially limited heat diffusion, the polymerization reaction is largely localized to the focus. This nonlinearity, similar to single-focus up-conversion-assisted VP[127,138,140] and 2PP, enables VP in a variety of thermally curing materials including opaque (to visible light) resins and ceramic composites[211]. Just as light can be controlled holographically by phase spatial light modulators (SLMs), phased arrays of ultrasound transducers or phase-plate holograms can produce 3D acoustic pressure fields. For now, the manipulation of particles and cells for directed assembly has motivated research into structured acoustic fields[212]. However, there is a clear synergy between these approaches, and it is likely that their convergence would enable novel in-situ multi-material assembly and volume-at-once patterning techniques. Furthermore, holographic ultrasound-directed assembly and localized heating could complement light-based tomographic VP enabling fascinating advances in tissue and composite engineering.

7. Conclusion and future perspectives

In this review, we have highlighted several VP techniques enabled by chemical and/or optical nonlinearity that have led to significant advances in printing rate, minimum feature size, and resolution. The progression from light-based printing at the surface to deep within a volume of photoresist carries with it many challenges involving the photochemical and optical behavior of the material. Furthermore, the characteristics of the photochemical mechanism from absorption of the photon/s to growth of the polymer network are tightly coupled with the physical properties of the material which vary both spatially and temporally during volumetric printing. Perhaps the

most pertinent example is that local change in viscosity associated with network growth and/or temperature change affects the diffusion rate of inhibitors employed to enhance chemical nonlinearity in tomographic VP and reduce parasitic initiation from intermediate metastable states in sequential absorption VP. In general, these links are complex and extensive trial-and-error is usually required to optimize printing conditions by identifying regimes where these effects are least consequential. Several reaction diffusion models have captured these relational properties in the context of 2PP[213–216]. However, multi-physics modelling efforts for emerging VP techniques have been limited and, when implemented, have often resorted to simplifications, such as, neglecting accumulation of light dose over time from tomographic projections. Not only do the changing physical properties of the photoresist affect the photochemical mechanism but, they can also distort the propagating light wavefront. We highlighted several distinct computational methods to simulate homogeneous scattering, refraction by axisymmetric aberrations, and absorption by opaque occlusions for tomographic VP. Ideally, a more general approach would be used, i.e., one that unifies all optical aberrations or non-idealities without employing disparate models to account for refraction at surfaces, refraction in smoothly varying refractive index distributions, scattering, and absorption separately and that supports time-varying effects like refractive index changes due to polymerization. As light-based 3D-printing evolves towards a volumetric volume-at-once process with resolution capabilities from nanoscale to the macroscale, the photophysical, chemical, and material dynamics naturally grow more complex. We expect that it will become increasingly important to be able to simulate the process with varying levels of fidelity from molecular simulations towards understanding complex polymerization dynamics[170,217] to

photochemical reaction-diffusion and optical propagation models to give the optimization of digital light projections a higher degree of fidelity.

Existing *in-situ* inspection techniques provide sufficient information to measure the evolution of the geometry and/or the refractive index of the printed object. To derive other properties relevant to the photopolymerization process, e.g., viscosity or modulus, temperature, and chemical species concentration, requires either an appropriate model relating the measured optical quantity to the desired physico-chemical property or extensive *ex-situ* characterization to relate the properties empirically. Alternative strategies drawing inspiration from fluorescence imaging in which a particular molecular probe responds to specific local material properties more directly could offer enhanced inspection capabilities to quantify evolving properties, reaction kinetics, and reaction products that are unmeasurable or confounded when measured with phase or scattering imaging modes[218–223]. Such an inspection strategy will be essential for validation of sophisticated multi-physics models.

VP, being light-based, non-contact, and not requiring relative material motion, enables unique combinations of different VP modalities and allows fabrication characteristics that none could achieve alone (at present). For example, tomographic VP offers massively parallelized photopolymerization at the macroscale with minimum feature size from 20–80 μm, whereas point-scanning multiphoton and UC-assisted photopolymerization achieves state-of-the-art sub-diffraction-limited minimum feature size and sub-micrometer resolution at high voxel production rate yet at lower volume production rate. Together, these optical volumetric photopolymerization modalities could produce unprecedented multiscale objects at high throughput. Two-photon ablation of microvascular channels inside previously tomographic VP-printed hydrogels hints at the utility that could be gained by incorporating 2PP in addition to subtractive machining. While

volumetric methods are the focus of this review, non-volumetric 3D-printing techniques have also converged with VP. The ability to print over or inside existing objects with optical VP means that direct extrusion-based methods can also participate. Several demonstrations including tomographic VP printing of hydrogels around melt-electrowritten skeletons and direct-ink-written cellular structures and UC-assisted direct write lithography around DLP-printed structures have already suggested the value of this synergy[55–57]. We expect that the perspective of viewing 3D-printing techniques, especially volumetric, as process modules which can be combined to capitalize on the best characteristics of each and form a process that is "greater than sum of its parts" will continue to generate products with superior functionality and cultivate meaningful collaborations between experts in different fields of 3D-printing.

Current advancements in VP have primarily focused on radical-mediated polymerizations, specifically involving (meth)acrylates and thiol-ene-based systems. While these chemistries have demonstrated considerable success in fabricating 3D objects via VP, it is anticipated that it will be important to extend the applicable chemistries to include non-radical chemistries, which will significantly broaden the scope of achievable material properties. Light-induced and radical-free uncaging of thiols through coumarin-based chromophores has illustrated this possibility by producing 3D objects via thiol-Michael-mediated 2PP[224]. Nucleophilic addition and substitution reactions as well as pericyclic reactions (i.e., Huisgen 1,3-dipolar cycloaddition, Diels-Alder) hold great promise for VP as a broad range of orthogonal click-chemistries exist that could be harnessed to create multi-material constructs, for example, in combination with radical-mediated polymerizations [225,226]. In particular, volume-at-once techniques such as tomographic VP, where the object is developed simultaneously, are well-suited for the implementation of relatively slow non-radical chemistries given the fact that only one unit

operation is needed to fabricate the entire 3D object. Several approaches can be considered to introduce the aforementioned chemistries to VP such as the use of photolabile protecting groups, photoacids/bases, or other photocatalysts that can catalyze the respective crosslinking reactions upon photoexcitation. However, it should be noted that some form of optical/chemical nonlinearity remains paramount to be applied in VP, making it a pivotal aspect for future research.

While the opportunities of the introduction of non-radical chemistries into VP are manyfold, one key advantage encompasses the ability to incorporate dynamic crosslinks, leading to 3D objects that are fully recyclable. By combining associative (i.e., vitrimers) or dissociative covalent adaptable networks with 3D-printing, it becomes possible to create objects that can undergo controlled depolymerization and reprocessing, enabling a more sustainable approach to manufacturing, paving the way towards exciting new avenues for material design and circular economy within the field of VP [227–229].

In the realm of VP, the significance of wavelength orthogonality and multi-material printing has been established. However, it is anticipated that this area will continue to be a focal point for future research. By manipulating additional wavelengths, the achievable complexity in the printed 3D objects can be significantly expanded. Implementation of spectral control (i.e., the ability of the incident color of light to tailor reactivity) is expected to be important, further building on pioneering principles including light-driven isomerization, deprotection, coupling, and electron/energy transfer[230]. Furthermore, the introduction of advanced photochemical schemes that rely on multiple wavelengths (including synergistic, orthogonal, and antagonistic photochemical schemes) is expected to play a crucial role in expanding the possibilities of spectral control in VP[231]. Carefully designing and orchestrating photochemical reactions that

rely on multiple wavelengths is expected to progress the field, enabling multi-material objects with advanced mechanical, optical and electrical properties.

The versatility of VP for 3D-printing of diverse polymers is abundantly clear, but the same cannot be said for 3D-printing inorganic materials. When incorporated as particles as they have commonly been in binder jetting and extrusion-based methods, inorganic materials present optical challenges in light-based VP. One approach, adjusting the refractive index of the photoresist to match that of the particle phase, has been successful for low index glasses but this only represents a small subset of desirable inorganic materials. Besides nanocomposites, polymer-derived ceramics and direct photo-reduction of metal salts dissolved in photoresists are routes to ceramic and metallic structures[232–235] without the potential of light scattering by a particle phase. However, the organic-inorganic hybrid photoresist approach has a limited scope because, for each inorganic material, a corresponding organic ligand and synthesis to combine the compounds must be optimized. The metal-salt solubility in organic photoresists requirement can be circumvented by employing a solvent exchange process to infuse previously printed polymer gel structures with a metal-salt solution[236]. In conjunction with adjustment of the photoexcitation wavelength or even utilizing non-light-based energy such as ultrasound to access favorable transmission in challenging composites and hybrid organic-inorganic photoresists, we anticipate that these approaches for printing inorganics can be extended to emerging VP techniques to further expand the gamut of processable materials.

Acknowledgements

Q.T. and S.V.V. would like to acknowledge funding from FWO (FWO-SB fellowship – 1SA2323N, EOS project 40007548) and Hercules I003922N. J.T. would like to thank the Mechanical Engineering Department for funding from a departmental fellowship. J.T. and H.T.

acknowledge funding from the National Science Foundation, under grant no. 2036849 and cooperative agreement no. EEC-1160494.

References

[1] Andre J-C, Mehaute AL, Witte OD. Dispositif pour realiser un modele de piece industrielle. FR2567668A1, 1986.

[2] Kodama H. Automatic method for fabricating a three-dimensional plastic model with photo-hardening polymer. Rev Sci Instrum 1981;52:1770–3. https://doi.org/10.1063/1.1136492.

[3] Hull CW. Apparatus for production of three-dimensional objects by stereolithography. US4575330A, 1986.

[4] Murphy CA, Lim KS, Woodfield TBF. Next Evolution in Organ-Scale Biofabrication: Bioresin Design for Rapid High-Resolution Vat Polymerization. Adv Mater 2022;34:e2107759. https://doi.org/10.1002/ADMA.202107759.

[5] Kessler A, Hickel R, Reymus M. 3D Printing in Dentistry—State of the Art. Oper Dent 2020;45:30–40. https://doi.org/10.2341/18-229-L.

[6] Bhattacharjee N, Urrios A, Kang S, Folch A. The upcoming 3D-printing revolution in microfluidics. Lab Chip 2016;16:1720–42. https://doi.org/10.1039/C6LC00163G.

[7] Matai I, Kaur G, Seyedsalehi A, McClinton A, Laurencin CT. Progress in 3D bioprinting technology for tissue/organ regenerative engineering. Biomaterials 2020;226:119536. https://doi.org/10.1016/j.biomaterials.2019.119536.

[8] Dickey MD. Stretchable and Soft Electronics using Liquid Metals. Adv Mater 2017;29:1606425. https://doi.org/10.1002/adma.201606425.

[9] Truby RL, Lewis JA. Printing soft matter in three dimensions. Nature 2016;540:371–8. https://doi.org/10.1038/nature21003.

[10] Surjadi JU, Gao L, Du H, Li X, Xiong X, Fang NX, et al. Mechanical Metamaterials and Their Engineering Applications. Adv Eng Mat 2019;21:1800864. https://doi.org/10.1002/adem.201800864.

[11] Gissibl T, Thiele S, Herkommer A, Giessen H. Two-photon direct laser writing of ultracompact multi-lens objectives. Nat Photonics 2016;10:554–60. https://doi.org/10.1038/nphoton.2016.121.

[12] Kuang X, Roach DJ, Wu J, Hamel CM, Ding Z, Wang T, et al. Advances in 4D Printing: Materials and Applications. Adv Funct Mater 2019;29:1805290. https://doi.org/10.1002/adfm.201805290.

[13] González-Henríquez CM, Sarabia-Vallejos MA, Rodriguez-Hernandez J. Polymers for additive manufacturing and 4D-printing: Materials, methodologies, and biomedical applications. Prog Polym Sci 2019;94:57–116. https://doi.org/10.1016/J.PROGPOLYMSCI.2019.03.001.

[14] Bagheri A. Application of RAFT in 3D Printing: Where Are the Future Opportunities? Macromolecules 2023;56:1778–97. https://doi.org/10.1021/acs.macromol.2c02585.

[15] Lee K, Corrigan N, Boyer C. Rapid High-Resolution 3D Printing and Surface Functionalization via Type I Photoinitiated RAFT Polymerization. Angew Chem Int Ed 2021;60:8839–50. https://doi.org/10.1002/anie.202016523.

[16] Kuang X, Wu J, Chen K, Zhao Z, Ding Z, Hu F, et al. Grayscale digital light processing 3D printing for highly functionally graded materials. Sci Adv 2019;5:eaav5790. https://doi.org/10.1126/sciadv.aav5790.

[17] Bagheri A, Jin J. Photopolymerization in 3D Printing. ACS Appl Polym Mater 2019;1:593–611. https://doi.org/10.1021/acsapm.8b00165

[18] Corrigan N, Yeow J, Judzewitsch P, Xu J, Boyer C. Seeing the Light: Advancing Materials Chemistry through Photopolymerization. Angew Chem Int Ed 2019;58:5170–89. https://doi.org/10.1002/ANIE.201805473.

[19] Lee M, Rizzo R, Surman F, Zenobi-Wong M. Guiding Lights: Tissue Bioprinting Using Photoactivated Materials. Chem Rev 2020;120:10950–1027. https://doi.org/10.1021/ACS.CHEMREV.0C00077.

[20] Xiao P, Zhang J, Dumur F, Tehfe MA, Morlet-Savary F, Graff B, et al. Visible light sensitive photoinitiating systems: Recent progress in cationic and radical photopolymerization reactions under soft conditions. Prog Polym Sci 2015;41:32–66. https://doi.org/10.1016/J.PROGPOLYMSCI.2014.09.001.

[21] Pan X, Tasdelen MA, Laun J, Junkers T, Yagci Y, Matyjaszewski K. Photomediated controlled radical polymerization. Prog Polym Sci 2016;62:73–125. https://doi.org/10.1016/J.PROGPOLYMSCI.2016.06.005.

[22] Andrzejewska E. Photopolymerization kinetics of multifunctional monomers.Prog Polym Sci 2001;26:605–65. https://doi.org/10.1016/S0079-6700(01)00004-1.

[23] Dietlin C, Schweizer S, Xiao P, Zhang J, Morlet-Savary F, Graff B, et al. Photopolymerization upon LEDs: new photoinitiating systems and strategies. Polym Chem 2015;6:3895–912. https://doi.org/10.1039/C5PY00258C.

[24] Zhao J, Wu W, Sun J, Guo S. Triplet photosensitizers: from molecular design to applications. Chem Soc Rev 2013;42:5323–51. https://doi.org/10.1039/C3CS35531D.

[25] Beljonne D, Shuai Z, Pourtois G, Bredas JL. Spin−Orbit Coupling and Intersystem Crossing in Conjugated Polymers: A Configuration Interaction Description.J Phys Chem A 2001;105:3899–907. https://doi.org/10.1021/jp010187w.

[26] Ligon SC, Husár B, Wutzel H, Holman R, Liska R. Strategies to reduce oxygen inhibition in photoinduced polymerization. Chem Rev 2014;114:577–89. https://doi.org/10.1021/cr3005197

[27] Barry JT, Berg DJ, Tyler DR. Radical Cage Effects: Comparison of Solvent Bulk Viscosity and Microviscosity in Predicting the Recombination Efficiencies of Radical Cage Pairs. J Am Chem Soc 2016;138:9389–92. https://doi.org/10.1021/jacs.6b05432.

[28] Tumbleston JR, Shirvanyants D, Ermoshkin N, Janusziewicz R, Johnson AR, Kelly DL, et al. Continuous liquid interface production of 3D objects. Science 2015;347:1349–52. https://doi.org/10.1126/science.aaa2397.

[29] Gabriel Lipkowitz, Tim Samuelsen, Hsiao K-W, Lee BJ, Dulay MT, Ian Coates, et al. Injection continuous liquid interface production of 3D objects. Sci Adv 2022;8:eabq3917. https://doi.org/10.1126/sciadv.abq3917.

[30] De Beer MP, Van Der Laan HL, Cole MA, Whelan RJ, Burns MA, Scott TF. Rapid, continuous additive manufacturing by volumetric polymerization inhibition patterning. Sci Adv 2019;5:eaau8723. https://doi.org/10.1126/sciadv.aau8723

[31] Walker DA, Hedrick JL, Mirkin CA. Rapid, large-volume, thermally controlled 3D printing using a mobile liquid interface. Science 2019;366:360–4. https://doi.org/10.1126/science.aax1562.

[32] Campbell M, Sharp DN, Harrison MT, Denning RG, Turberfield AJ. Fabrication of photonic crystals for the visible spectrum by holographic lithography. Nature 2000;404:53–6.https://doi.org/10.1038/35003523.

[33] Jang J -H., Ullal CK, Maldovan M, Gorishnyy T, Kooi S, Koh C, et al. 3D Micro- and Nanostructures via Interference Lithography. Adv Funct Mater 2007;17:3027–41. https://doi.org/10.1002/adfm.200700140.

[34] Shusteff M, Browar AEM, Kelly BE, Henriksson J, Weisgraber TH, Panas RM, et al. One-step volumetric additive manufacturing of complex polymer structures. Sci Adv 2017;3:eaao5496. https://doi.org/10.1126/sciadv.aao5496

[35] Kelly BE, Bhattacharya I, Shusteff M, Taylor HK, Spadaccini CM. Computed Axial Lithography For Rapid Volumetric 3D Additive Manufacturing. Proceedings of the 28th Annual International Solid Freeform Fabrication Symposium 2017:938–50. https://utw10945.utweb.utexas.edu/sites/default/files/2017/Manuscripts/ComputedAxialLithographyforRapidVolumetric3D.pdf

[36] Kelly BE, Bhattacharya I, Heidari H, Shusteff M, Spadaccini CM, Taylor HK. Volumetric additive manufacturing via tomographic reconstruction. Science 2019;363:1075–9. https://doi.org/10.1126/science.aau7114.

[37] Loterie D, Delrot P, Moser C. High-resolution tomographic volumetric additive manufacturing. Nat Commun 2020;11:1–6. https://doi.org/10.1038/s41467-020-14630-4.

[38] Cook CC, Fong EJ, Schwartz JJ, Porcincula DH, Kaczmarek AC, Oakdale JS, et al. Highly Tunable Thiol-Ene Photoresins for Volumetric Additive Manufacturing. Adv Mater 2020;32:2003376. https://doi.org/10.1002/ADMA.202003376.

[39] Schwartz JJ, Porcincula DH, Cook CC, Fong EJ, Shusteff M. Volumetric additive manufacturing of shape memory polymers. Polym Chem 2022;13:1813–7. https://doi.org/10.1039/D1PY01723C.

[40] Wang B, Engay E, Stubbe PR, Moghaddam SZ, Thormann E, Almdal K, et al. Stiffness control in dual color tomographic volumetric 3D printing. Nat Commun 2022;13:367. https://doi.org/10.1038/s41467-022-28013-4.

[41] Chansoria P, Rütsche D, Wang A, Liu H, D'Angella D, Rizzo R, et al. Synergizing Algorithmic Design, Photoclick Chemistry and Multi-Material Volumetric Printing for Accelerating Complex Shape Engineering. Adv Sci 2023;10:2300912. https://doi.org/10.1002/advs.202300912.

[42] Soliman BG, Longoni A, Wang M, Li W, Bernal PN, Cianciosi A, et al. Programming Delayed Dissolution Into Sacrificial Bioinks For Dynamic Temporal Control of Architecture within 3D-Bioprinted Constructs. Adv Func Mater 2023;33:2210521. https://doi.org/10.1002/ADFM.202210521.

[43] Toombs JT, Luitz M, Cook CC, Jenne S, Li CC, Rapp BE, et al. Volumetric additive manufacturing of silica glass with microscale computed axial lithography. Science 2022;376:308–12. https://doi.org/10.1126/science.abm6459

[44] Kollep M, Konstantinou G, Madrid-Wolff J, Boniface A, Hagelüken L, Sasikumar PVW, et al. Tomographic Volumetric Additive Manufacturing of Silicon Oxycarbide

Ceramics. Adv Eng Mater 2022;24:2101345. https://doi.org/10.1002/ADEM.202101345.

[45] Thijssen Q, Quaak A, Toombs J, Vlieghere ED, Parmentier L, Taylor H, et al. Volumetric Printing of Thiol-Ene Photo-Cross-Linkable Poly(ϵ-caprolactone): a Tunable Material Platform serving Biomedical Applications. Adv Mater 2023;35:e2210136. https://doi.org/10.1002/ADMA.202210136.

[46] Bernal PN, Delrot P, Loterie D, Li Y, Malda J, Moser C, et al. Volumetric Bioprinting of Complex Living-Tissue Constructs within Seconds. Adv Mater 2019;31:e2110054. https://doi.org/10.1002/adma.201904209.

[47] Bernal PN, Bouwmeester M, Madrid-Wolff J, Falandt M, Florczak S, Rodriguez NG, et al. Volumetric Bioprinting of Organoids and Optically Tuned Hydrogels to Build Liver-Like Metabolic Biofactories. Adv Mater 2022;34:e2110054. https://doi.org/10.1002/adma.202110054.

[48] Gehlen J, Qiu W, Schädli GN, Müller R, Qin XH. Tomographic volumetric bioprinting of heterocellular bone-like tissues in seconds. Acta Biomater 2023;156:49–60. https://doi.org/10.1016/J.ACTBIO.2022.06.020.

[49] Rizzo R, Rütsche D, Dominic Ruetsche, Liu H, Hao Liu, Zenobi-Wong M. Optimized Photoclick (Bio)Resins for Fast Volumetric Bioprinting. Adv Mater 2021;33:2102900. https://doi.org/10.1002/adma.202102900.

[50] Luo T, Tan B, Zhu L, Wang Y, Liao J. A Review on the Design of Hydrogels With Different Stiffness and Their Effects on Tissue Repair. Front Bioeng Biotech 2022;10:817391. https://doi.org/10.3389/fbioe.2022.817391.

[51] Xie M, Lian L, Mu X, Luo Z, Garciamendez-Mijares CE, Zhang Z, et al. Volumetric additive manufacturing of pristine silk-based (bio)inks. Nat Commun 2023;14:210. https://doi.org/10.1038/s41467-023-35807-7.

[52] Qiu W, Gehlen J, Bernero M, Gehre C, Schädli GN, Müller R, et al. A Synthetic Dynamic Polyvinyl Alcohol Photoresin for Fast Volumetric Bioprinting of Functional Ultrasoft Hydrogel Constructs. Adv Funct Mater 2023;33:2214393. https://doi.org/10.1002/ADFM.202214393.

[53] Falandt M, Bernal PN, Dudaryeva O, Florczak S, Größbacher G, Schweiger M, et al. Spatial-Selective Volumetric 4D Printing and Single-Photon Grafting of Biomolecules within Centimeter-Scale Hydrogels via Tomographic Manufacturing. Adv Mater Technol 23;8:2300026.https://doi.org/10.1002/admt.202300026.

[54] Rodríguez-Pombo L, Martínez-Castro L, Xu X, Ong JJ, Rial C, García DN, et al. Simultaneous fabrication of multiple tablets within seconds using tomographic volumetric 3D printing. Int J Pharm: X 2023;5:100166. https://doi.org/10.1016/J.IJPX.2023.100166.

[55] Rizzo R, Rütsche D, Liu H, Chansoria P, Wang A, Hasenauer A, et al. Multiscale Hybrid Fabrication: Volumetric Printing Meets Two-Photon Ablation. Adv Mater Technol 2023;8:2201871. https://doi.org/10.1002/admt.202201871.

[56] Größbacher G, Bartolf-Kopp M, Gergely C, Bernal PN, Florczak S, de Ruijter M, et al. Volumetric Printing across Melt Electrowritten Scaffolds Fabricates Multi-Material Living Constructs with Tunable Architecture and Mechanics. Adv Mater 2023;35:e2300756. https://doi.org/10.1002/adma.202300756.

[57] Ribezzi D, Gueye M, Florczak S, Dusi F, De Vos D, Manente F, et al. Shaping Synthetic Multicellular and Complex Multimaterial Tissues via Embedded Extrusion-Volumetric Printing of Microgels. Adv Mater 2023;35:2301673. https://doi.org/10.1002/adma.202301673.

[58] Madrid-Wolff J, Toombs J, Rizzo R, Bernal PN, Porcincula D, Walton R, et al. A review of materials used in tomographic volumetric additive manufacturing. MRS Commun 2023. https://doi.org/10.1557/s43579-023-00447-x.

[59] Terenziani F, Katan C, Badaeva E, Tretiak S, Blanchard-Desce M. Enhanced Two-Photon Absorption of Organic Chromophores: Theoretical and Experimental Assessments. Adv Mater 2008;20:4641–78.https://doi.org/10.1002/adma.200800402.

[60] So PTC, Dong CY, Masters BR, Berland KM. Two-Photon Excitation Fluorescence Microscopy. Annu Rev Biomed Eng 2000;2:399–429. https://doi.org/10.1146/annurev.bioeng.2.1.399.

[61] Oron D, Papagiakoumou E, Anselmi F, Emiliani V. Two-photon optogenetics. Prog Brain Res 2012;196:119–43. https://doi.org/10.1016/B978-0-444-59426-6.00007-0.

[62] Asshauer T, Latz C, Mirshahi A, Rathjen C. Femtosecond lasers for eye surgery applications: historical overview and modern low pulse energy concepts. Adv Opt Technol 2021;10:393–408. https://doi.org/10.1515/aot-2021-0044.

[63] Lee K-S, Kim RH, Yang D-Y, Park SH. Advances in 3D nano/microfabrication using two-photon initiated polymerization. Prog Polym Sci 2008;33:631–81. https://doi.org/10.1016/j.progpolymsci.2008.01.001.

[64] Gonzalez-Hernandez D, Varapnickas S, Bertoncini A, Liberale C, Malinauskas M. Micro-Optics 3D Printed via Multi-Photon Laser Lithography. Adv Opt Mater 2023;11:2201701. https://doi.org/10.1002/adom.202201701.

[65] Huang Z, Chi-Pong Tsui G, Deng Y, Tang C-Y. Two-photon polymerization nanolithography technology for fabrication of stimulus-responsive micro/nano-structures for biomedical applications. Nanotechnol 2020;9:1118–36. https://doi.org/10.1515/ntrev-2020-0073.

[66] Torgersen J, Qin X-H, Li Z, Ovsianikov A, Liska R, Stampfl J. Hydrogels for Two-Photon Polymerization: A Toolbox for Mimicking the Extracellular Matrix. Adv Funct Mater 2013;23:4542–54. https://doi.org/10.1002/adfm.201203880.

[67] Soukoulis CM, Wegener M. Past achievements and future challenges in the development of three-dimensional photonic metamaterials. Nat Photonics 2011;5:523–30. https://doi.org/10.1038/nphoton.2011.154.

[68] Kadic M, Milton GW, van Hecke M, Wegener M. 3D metamaterials. Nat Rev Phys 2019;1:198–210. https://doi.org/10.1038/s42254-018-0018-y.

[69] Su R, Chen J, Zhang X, Wang W, Li Y, He R, et al. 3D-Printed Micro/Nano-Scaled Mechanical Metamaterials: Fundamentals, Technologies, Progress, Applications, and Challenges. Small 2023;19:2206391. https://doi.org/10.1002/smll.202206391.

[70] Farsari M, Filippidis G, Fotakis C. Fabrication of three-dimensional structures by three-photon polymerization. Opt Lett 2005;30:3180. https://doi.org/10.1364/ol.30.003180.

[71] Balena A, Bianco M, Pisanello F, De Vittorio M. Recent Advances on High-Speed and Holographic Two-Photon Direct Laser Writing. Adv Funct Mater 2023;33:2211773. https://doi.org/10.1002/adfm.202211773.

[72] Hahn V, Kiefer P, Frenzel T, Qu J, Blasco E, Barner-Kowollik C, et al. Rapid Assembly of Small Materials Building Blocks (Voxels) into Large Functional 3D Metamaterials. Adv Funct Mater 2020;30:1907795. https://doi.org/10.1002/adfm.201907795.

[73] Pearre BW, Michas C, Tsang JM, Gardner TJ, Otchy TM. Fast micron-scale 3D printing with a resonant-scanning two-photon microscope. Addit Manuf 2019;30:100887. https://doi.org/10.1016/j.addma.2019.100887.

[74] Rensch C, Hell S, Schickfus M v., Hunklinger S. Laser scanner for direct writing lithography. Appl Opt 1989;28:3754. https://doi.org/10.1364/AO.28.003754.

[75] Jiao BJ, Chen F, Liu Y, Fan X, Zeng S, Dong Q, et al. Acousto-optic Scanning Spatial-switching Multiphoton Lithography. Int J Extrem Manuf 2023;5:035008. https://doi.org/10.1088/2631-7990/ace0a7.

[76] Kato J-I, Takeyasu N, Adachi Y, Sun H-B, Kawata S. Multiple-spot parallel processing for laser micronanofabrication. Appl Phys Lett 2005;86:044102. https://doi.org/10.1063/1.1855404.

[77] Yang S, Su C, Gu S, Sun Q, Sun Q, Xu L, et al. Parallel two-photon lithography achieving uniform sub-200 nm features with thousands of individually controlled foci. Opt Express 2023;31:14174. https://doi.org/10.1364/OE.483524.

[78] Dong X-Z, Zhao Z-S, Duan X-M. Micronanofabrication of assembled three-dimensional microstructures by designable multiple beams multiphoton processing. Appl Phys Lett 2007;91:124103. https://doi.org/10.1063/1.2789661.

[79] Trautmann A, Rüth M, Lemke HD, Walther T, Hellmann R. Two-photon polymerization based large scaffolds for adhesion and proliferation studies of human primary fibroblasts. Opt Laser Technol 2018;106:474–80. https://doi.org/10.1016/j.optlastec.2018.05.008.

[80] Maibohm C, Silvestre OF, Borme J, Sinou M, Heggarty K, Nieder JB. Multi-beam two-photon polymerization for fast large area 3D periodic structure fabrication for bioapplications.Sci Rep 2020;10:1–10. https://doi.org/10.1038/s41598-020-64955-9.

[81] Geng Q, Wang D, Chen P, Chen S-C. Ultrafast multi-focus 3-D nano-fabrication based on two-photon polymerization. Nat Commun 2019;10:2179. https://doi.org/10.1038/s41467-019-10249-2.

[82] Ouyang W, Xu X, Lu W, Zhao N, Han F, Chen S-C. Ultrafast 3D nanofabrication via digital holography. Nat Commun 2023;14:1716. https://doi.org/10.1038/s41467-023-37163-y.

[83] Zhang SJ, Li Y, Liu ZP, Ren JL, Xiao YF, Yang H, et al. Two-photon polymerization of a three dimensional structure using beams with orbital angular momentum. Appl Phys Lett 2014;105:061101. https://doi.org/10.1063/1.4893007.

[84] Yang D, Liu L, Gong Q, Li Y. Rapid Two-Photon Polymerization of an Arbitrary 3D Microstructure with 3D Focal Field Engineering. Macromol Rapid Commun 2019;40:1–4. https://doi.org/10.1002/marc.201900041.

[85] Saha SK, Wang D, Nguyen VH, Chang Y, Oakdale JS, Chen S-C. Scalable submicrometer additive manufacturing. Science 2019;366:105–9. https://doi.org/10.1126/science.aax8760.

[86] Somers P, Liang Z, Johnson JE, Boudouris BW, Pan L, Xu X. Rapid, continuous projection multi-photon 3D printing enabled by spatiotemporal focusing of femtosecond pulses. Light Sci Appl 2021;10:199. https://doi.org/10.1038/s41377-021-00645-z.

[87] Yan L, Yang D, Gong Q, Li Y. Rapid fabrication of continuous surface fresnel microlens array by femtosecond laser focal field engineering. Micromachines 2020;11:112. https://doi.org/10.3390/mi11020112.

[88] Wang C, Yang L, Hu Y, Rao S, Wang Y, Pan D, et al. Femtosecond Mathieu Beams for Rapid Controllable Fabrication of Complex Microcages and Application in Trapping Microobjects. ACS Nano 2019;13:4667–76.https://doi.org/10.1021/acsnano.9b00893.

[89] Barner-Kowollik C, Bastmeyer M, Blasco E, Delaittre G, Müller P, Richter B, et al. 3D Laser Micro- and Nanoprinting: Challenges for Chemistry. Angew Chem Int Ed 2017;56:15828–45. https://doi.org/10.1002/anie.201704695.

[90] Wloka T, Gottschaldt M, Schubert US. From Light to Structure: Photo Initiators for Radical Two-Photon Polymerization. Chem Eur J 2022;28:e202104191. https://doi.org/10.1002/chem.202104191.

[91] Chi T, Somers P, Wilcox DA, Schuman AJ, Iyer V, Le R, et al. Tailored thioxanthone-based photoinitiators for two-photon-controllable polymerization and nanolithographic printing. J Polym Sci Part B: Polym Phys 2019;57:1462–75. https://doi.org/10.1002/polb.24891.

[92] Holzer B, Lunzer M, Rosspeintner A, Licari G, Tromayer M, Naumov S, et al. Towards efficient initiators for two-photon induced polymerization: fine tuning of the donor/acceptor properties. Mol Syst Des Eng 2019;4:437–48. https://doi.org/10.1039/C8ME00101D.

[93] Tang J, Xu X, Shen X, Kuang C, Chen H, Shi M, et al. Ketocoumarin-Based Photoinitiators for High-Sensitivity Two-Photon Lithography. ACS Appl Polym Mater 2023;5:2956-63. https://doi.org/10.1021/acsapm.3c00141.

[94] Whitby R, Ben-Tal Y, MacMillan R, Janssens S, Raymond S, Clarke D, et al. Photoinitiators for two-photon polymerisation: effect of branching and viscosity on polymerisation thresholds. RSC Adv 2017;7:13232–9. https://doi.org/10.1039/C6RA27176F.

[95] Lunzer M, Beckwith JS, Chalupa-Gantner F, Rosspeintner A, Licari G, Steiger W, et al. Beyond the Threshold: A Study of Chalcogenophene-Based Two-Photon Initiators. Chem Mater 2022;34:3042–52. https://doi.org/10.1021/acs.chemmater.1c04002.

[96] Arnoux C, Konishi T, Van Elslande E, Poutougnigni E-A, Mulatier J-C, Khrouz L, et al. Polymerization Photoinitiators with Near-Resonance Enhanced Two-Photon Absorption Cross-Section: Toward High-Resolution Photoresist with Improved Sensitivity. Macromolecules 2020;53:9264–78. https://doi.org/10.1021/acs.macromol.0c01518.

[97] Bonačić-Koutecký V, Antoine R. Enhanced two-photon absorption of ligated silver and gold nanoclusters: theoretical and experimental assessments. Nanoscale 2019;11:12436–48. https://doi.org/10.1039/C9NR01826C.

[98] Olesiak-Banska J, Waszkielewicz M, Obstarczyk P, Samoc M. Two-photon absorption and photoluminescence of colloidal gold nanoparticles and nanoclusters. Chem Soc Rev 2019;48:4087–117. https://doi.org/10.1039/C8CS00849C.

[99] Ramakrishna G, Varnavski O, Kim J, Lee D, Goodson T. Quantum-Sized Gold Clusters as Efficient Two-Photon Absorbers. J Am Chem Soc 2008;130:5032–3. https://doi.org/10.1021/ja800341v.

[100] Olesiak-Banska J, Waszkielewicz M, Matczyszyn K, Samoc M. A closer look at two-photon absorption, absorption saturation and nonlinear refraction in gold nanoclusters. RSC Adv 2016;6:98748–52. https://doi.org/10.1039/C6RA20610G.

[101] Hu Z, Jensen L.Importance of double-resonance effects in two-photon absorption properties of $Au_{25}(SR)_{18}^{-}$. Chem Sci 2017;8:4595–601. https://doi.org/10.1039/C7SC00968B.

[102] Li Q, Kulikowski J, Doan D, Tertuliano OA, Zeman CJ, Wang MM, et al. Mechanical nanolattices printed using nanocluster-based photoresists. Science 2022;378:768–73. https://doi.org/10.1126/science.abo6997.

[103] Kiefer P, Hahn V, Nardi M, Yang L, Blasco E, Barner-Kowollik C, et al. Sensitive Photoresists for Rapid Multiphoton 3D Laser Micro- and Nanoprinting. Adv Opt Mater 2020;8:2000895. https://doi.org/10.1002/adom.202000895.

[104] Shinohara M, Ushida T, Furukawa KS. Design and Development of In-Process-Resolution-Tunable Stereolithography (iPRT) System Utilizing Two- Photon Polymerization.Adv Eng Mater 2023:202300122. https://doi.org/10.1002/adem.202300122.

[105] Hahn V, Rietz P, Hermann F, Müller P, Barner-Kowollik C, Schlöder T, et al. Light-sheet 3D microprinting via two-colour two-step absorption. Nat Photonics 2022;16:784–91. https://doi.org/10.1038/s41566-022-01081-0.

[106] Brauchle Chr, Wild UP, Burland DM, Bjorklund GC, Alvarez DC. A New Class of Materials for Holography in the Infrared. IBM J Res Dev 1982;26:217–27. https://doi.org/10.1147/rd.262.0217.

[107] Bräuchle Chr, Wild UP, Burland DM, Bjorklund GC, Alvarez DC. Two-photon holographic recording with continuous-wave lasers in the 750–1100-nm range. Opt Lett 1982;7:177. https://doi.org/10.1364/OL.7.000177.

[108] Hahn V, Messer T, Bojanowski NM, Curticean ER, Wacker I, Schröder RR, et al. Two-step absorption instead of two-photon absorption in 3D nanoprinting. Nat Photonics 2021;15:932–8. https://doi.org/10.1038/s41566-021-00906-8.

[109] Fang T-S, Brown RE, Kwan CL, Singer LA. Photophysical studies on benzil. Time resolution of the prompt and delayed emissions and a photokinetic study indicating deactivation of the triplet by reversible exciplex formation. J Phys Chem 1978;82:2489–96. https://doi.org/10.1021/j100512a008.

[110] Bojanowski NM, Vranic A, Hahn V, Rietz P, Messer T, Brückel J, et al. Search for Alternative Two-Step-Absorption Photoinitiators for 3D Laser Nanoprinting. Adv Funct Mater 2022;33:2212482. https://doi.org/10.1002/adfm.202212482.

[111] Shimizu M, Schelper M, Mochida K, Hiyama T, Adachi M, Sasaki Y, et al. A Novel Strategy for Two-Photon Holographic Recording: Stepwise Two-Photon Absorption of α-Quinquethiophene Followed by Energy Transfer to an Aryl Azide. Adv Mater 2007;19:1826–9. https://doi.org/10.1002/adma.200700432.

[112] Kobayashi Y, Mutoh K, Abe J. Stepwise two-photon absorption processes utilizing photochromic reactions. J Photochem Photobiol C: Photochem Rev 2018;34:2–28. https://doi.org/10.1016/j.jphotochemrev.2017.12.006.

[113] Goulet-Hanssens A, Eisenreich F, Hecht S. Enlightening Materials with Photoswitches. Adv Mater 2020;32:1905966.https://doi.org/10.1002/adma.201905966.

[114] Jeudy MJ, Robillard JJ. Spectral photosensitization of a variable index material for recording phase holograms with high efficiency. Opt Commun 1975;13:25–8. https://doi.org/10.1016/0030-4018(75)90149-2.

[115] Lee SK, Neckers DC. Two-photon radical-photoinitiator system based on iodinated benzospiropyrans. Chem Mater 1991;3:858–64. https://doi.org/10.1021/cm00017a022.

[116] Regehly M, Garmshausen Y, Reuter M, König NF, Israel E, Kelly DP, et al. Xolography for linear volumetric 3D printing. Nature 2020;588:620–4. https://doi.org/10.1038/s41586-020-3029-7.

[117] Stüwe L, Geiger M, Röllgen F, Heinze T, Reuter M, Wessling M, et al. Continuous Volumetric 3D Printing: Xolography in Flow.Adv Mater 2023:2306716. https://doi.org/10.1002/adma.202306716.

[118] Sousa CM, Fernandes JR, Coelho PJ. Naphthopyrans as efficient dual color photoinitiators for volumetric 3D printing. Eur Polym J 2023;196:112312. https://doi.org/10.1016/j.eurpolymj.2023.112312.

[119] Ichimura K, Sakuragi M. A spiropyran-iodonium salt system as a two photon radical photoinitiator. J Polym Sci Polym Lett Ed 1988;26:185–9. https://doi.org/10.1002/pol.1988.140260403.

[120] Auzel F. Upconversion and Anti-Stokes Processes with f and d Ions in Solids. Chem Rev 2004;104:139–74. https://doi.org/10.1021/cr020357g.

[121] Chen G, Qiu H, Prasad PN, Chen X. Upconversion Nanoparticles: Design, Nanochemistry, and Applications in Theranostics. Chem Rev 2014;114:5161–214. https://doi.org/10.1021/cr400425h.

[122] Schloemer T, Narayanan P, Zhou Q, Belliveau E, Seitz M, Congreve DN. Nanoengineering Triplet–Triplet Annihilation Upconversion: From Materials to Real-World Applications. ACS Nano 2023;17:3259–88. https://doi.org/10.1021/acsnano.3c00543.

[123] Wang K, Peña J, Xing J. Upconversion Nanoparticle-Assisted Photopolymerization. Photochem Photobiol 2020;96:741–9. https://doi.org/10.1111/php.13249.

[124] Wang F, Liu X. Recent advances in the chemistry of lanthanide-doped upconversion nanocrystals. Chem Soc Rev 2009;38:976. https://doi.org/10.1039/b809132n.

[125] Nadort A, Zhao J, Goldys EM. Lanthanide upconversion luminescence at the nanoscale: fundamentals and optical properties. Nanoscale 2016;8:13099–130. https://doi.org/10.1039/C5NR08477F.

[126] Duan C, Liang L, Li L, Zhang R, Xu ZP. Recent progress in upconversion luminescence nanomaterials for biomedical applications. J Mater Chem B 2018;6:192–209. https://doi.org/10.1039/C7TB02527K.

[127] Sanders SN, Schloemer TH, Gangishetty MK, Anderson D, Seitz M, Gallegos AO, et al. Triplet fusion upconversion nanocapsules for volumetric 3D printing. Nature 2022;604:474–8. https://doi.org/10.1038/s41586-022-04485-8.

[128] Dika I, Malval J-P, Soppera O, Bardinal V, Barat D, Turck C, et al. Near-infrared photopolymerization: Initiation process assisted by self-quenching and triplet–triplet annihilation of excited cyanine dyes. Chem Phys Lett 2011;515:91–5. https://doi.org/10.1016/j.cplett.2011.08.091.

[129] Kang J-H, Reichmanis E. Low-Threshold Photon Upconversion Capsules Obtained by Photoinduced Interfacial Polymerization. Angew Chem Int Ed 2012;51:11841–4. https://doi.org/10.1002/anie.201205540.

[130] Awwad N, Bui AT, Danilov EO, Castellano FN. Visible-Light-Initiated Free-Radical Polymerization by Homomolecular Triplet-Triplet Annihilation. Chem 2020;6:3071–85. https://doi.org/10.1016/j.chempr.2020.08.019.

[131] Singh-Rachford TN, Castellano FN. Photon upconversion based on sensitized triplet–triplet annihilation. Coord Chem Rev 2010;254:2560–73. https://doi.org/10.1016/j.ccr.2010.01.003.

[132] Wang X, Valiev RR, Ohulchanskyy TY, Ågren H, Yang C, Chen G.Dye-sensitized lanthanide-doped upconversion nanoparticles. Chem Soc Rev 2017;46:4150–67. https://doi.org/10.1039/C7CS00053G.

[133] Forecast R, Campaioli F, Schmidt TW, Cole JH. Photochemical Upconversion in Solution: The Role of Oxygen and Magnetic Field Response. J Phys Chem A 2023;127:1794–800. https://doi.org/10.1021/acs.jpca.2c08883.

[134] Schloemer TH, Sanders SN, Narayanan P, Zhou Q, Hu M, Congreve DN. Controlling the durability and optical properties of triplet–triplet annihilation upconversion nanocapsules. Nanoscale 2023;15:6880–9. https://doi.org/10.1039/D3NR00067B.

[135] Liu R, Chen H, Li Z, Shi F, Liu X. Extremely deep photopolymerization using upconversion particles as internal lamps. Polym Chem 2016;7:2457–63. https://doi.org/10.1039/C6PY00184J.

[136] Darani MK, Bastani S, Ghahari M, Kardar P, Mohajerani E. NIR induced photopolymerization of acrylate-based composite containing upconversion particles as an internal miniaturized UV sources. Prog Org Coat 2017;104:97–103. https://doi.org/10.1016/j.porgcoat.2016.11.005.

[137] Chen Y, Zhang J, Liu X, Wang S, Tao J, Huang Y, et al. Noninvasive in vivo 3D bioprinting. Sci Adv 2020;6:eaba7406. https://doi.org/10.1126/sciadv.aba7406.

[138] Limberg DK, Kang J-H, Hayward RC. Triplet–Triplet Annihilation Photopolymerization for High-Resolution 3D Printing. J Am Chem Soc 2022;144:5226–32. https://doi.org/10.1021/jacs.1c11022.

[139] Wang Z, Zhang Y, Su Y, Zhang C, Wang C. Three-dimensional direct-writing via photopolymerization based on triplet—triplet annihilation. Sci China Chem 2022;65:2283–9. https://doi.org/10.1007/s11426-022-1380-6.

[140] Zhang Q, Boniface A, Parashar VK, Gijs MAM, Moser C. Multi-photon polymerization using upconversion nanoparticles for tunable feature-size printing. Nanophotonics 2023;12:1527-36. https://doi.org/10.1515/nanoph-2022-0598.

[141] Luo Z, Wang D, Li K, Zhong D, Xue L, Gan Z, et al. Three-Dimensional Nanolithography with Visible Continuous Wave Laser through Triplet Up-Conversion. J Phys Chem Lett 2023;14:709–15. https://doi.org/10.1021/acs.jpclett.2c03601.

[142] Rocheva VV, Koroleva AV, Savelyev AG, Khaydukov KV, Generalova AN, Nechaev AV, et al. High-resolution 3D photopolymerization assisted by upconversion

nanoparticles for rapid prototyping applications. Sci Rep 2018;8:3663. https://doi.org/10.1038/s41598-018-21793-0.

[143] Park W, Lu D, Ahn S. Plasmon enhancement of luminescence upconversion. Chem Soc Rev 2015;44:2940–62. https://doi.org/10.1039/C5CS00050E.

[144] Lu D, Mao C, Cho SK, Ahn S, Park W. Experimental demonstration of plasmon enhanced energy transfer rate in NaYF4:Yb3+,Er3+ upconversion nanoparticles. Sci Rep 2016;6:18894. https://doi.org/10.1038/srep18894.

[145] Das A, Mao C, Cho S, Kim K, Park W. Over 1000-fold enhancement of upconversion luminescence using water-dispersible metal-insulator-metal nanostructures. Nat Commun 2018;9:4828. https://doi.org/10.1038/s41467-018-07284-w.

[146] Dong J, Gao W, Han Q, Wang Y, Qi J, Yan X, et al. Plasmon-enhanced upconversion photoluminescence: Mechanism and application. Rev Phys 2019;4:100026. https://doi.org/10.1016/j.revip.2018.100026.

[147] Oprych D, Schmitz C, Ley C, Allonas X, Ermilov E, Erdmann R, et al. Photophysics of Up-Conversion Nanoparticles: Radical Photopolymerization of Multifunctional Methacrylates Comprising Blue- and UV-Sensitive Photoinitiators. ChemPhotoChem 2019;3:1119–26. https://doi.org/10.1002/cptc.201900196.

[148] Li Z, Zou X, Shi F, Liu R, Yagci Y. Highly efficient dandelion-like near-infrared light photoinitiator for free radical and thiol-ene photopolymerizations. Nat Commun 2019;10:3560. https://doi.org/10.1038/s41467-019-11522-0.

[149] Maruo S, Nakamura O, Kawata S. Three-dimensional microfabrication with two-photon-absorbed photopolymerization. Opt Lett 1997;22:132–4. https://doi.org/10.1364/OL.22.000132.

[150] Maruo S, Ikuta K. Three-dimensional microfabrication by use of single-photon-absorbed polymerization. Appl Phys Lett 2000;76:2656–8. https://doi.org/10.1063/1.126742.

[151] Hsu S, Chi T, Kim J, Somers P, Boudouris BW, Xu X, et al. High-Speed One-Photon 3D Nanolithography Using Controlled Initiator Depletion and Inhibitor Transport. Adv Opt Mater 2022;10:2102262. https://doi.org/10.1002/adom.202102262.

[152] Orth A, Webber D, Zhang Y, Sampson KL, de Haan HW, Lacelle T, et al. Deconvolution volumetric additive manufacturing. Nat Commun 2023;14:4412. https://doi.org/10.1038/s41467-023-39886-4.

[153] He M, Zhang Z, Cao C, Zhou G, Kuang C, Liu X. 3D Sub-Diffraction Printing by Multicolor Photoinhibition Lithography: From Optics to Chemistry. Laser Photonics Rev 2022;16:2100229. https://doi.org/10.1002/LPOR.202100229.

[154] Sakellari I, Kabouraki E, Gray D, Purlys V, Fotakis C, Pikulin A, et al. Diffusion-Assisted High-Resolution Direct Femtosecond Laser Writing. ACS Nano 2012;6:2302–11. https://doi.org/10.1021/nn204454c.

[155] Pazos JF. Photopolymerizable composition containing an o-nitroaromatic compound as photoinhibitor. US4198242A, 1980.

[156] Dueber TE, Nebe WJ. Acidic o-nitroaromatics as photoinhibitors of polymerization in positive working films. US4477556A, 1984.

[157] Scott TF, Kowalski BA, Sullivan AC, Bowman CN, McLeod RR. Two-Color Single-Photon Photoinitiation and Photoinhibition for Subdiffraction Photolithography. Science 2009;324:913–7. https://doi.org/10.1126/science.1167610.

[158] Forman DL, McLeod RR. Photoinhibited superresolution lithography: overcoming chemical blur. Proceedings SPIE 9049, Alternative Lithographic Technologies VI, 90491W (28 March 2014). https://doi.org/10.1117/12.2063254.

[159] Forman DL, Cole MC, McLeod RR. Radical diffusion limits to photoinhibited superresolution lithography. Phys Chem Chem Phys 2013;15:14862. https://doi.org/10.1039/c3cp51512e.

[160] Wang B, Sun W, Narag JPC, Mozajin HS, Christiansen TDV, Frisvad JR, et al. Creating negative illumination for tomographic 3D printing via binary photoinhibition arXiv 2023;2303.13941 https://doi.org/10.48550/arXiv.2303.13941.

[161] van der Laan HL, Burns MA, Scott TF. Volumetric Photopolymerization Confinement through Dual-Wavelength Photoinitiation and Photoinhibition. ACS Macro Lett 2019;8:899–904. https://doi.org/10.1021/acsmacrolett.9b00412.

[162] Berdzinski S, Strehmel N, Lindauer H, Strehmel V, Strehmel B. Extended mechanistic aspects on photoinitiated polymerization of 1,6-hexanediol diacrylate by hexaarylbisimidazoles and heterocyclic mercapto compounds. Photochem Photobiol Sci 2014;13:789–98. https://doi.org/10.1039/c3pp50379h.

[163] Zhu QQ, Fink M, Seitz F, Schneider S, Schnabel W. On the photolysis of bis[2-(o-chlorophenyl)-4,5-diphenylimidazole] sensitized by 2-isopropylthioxanthone or Michler's ketone. J Photochem Photobiol A Chem 1991;59:255–63. https://doi.org/10.1016/1010-6030(91)87013-L.

[164] Kowalski BA, Scott TF, Bowman CN, Sullivan AC, McLeod RR. Exceeding the diffraction limit with single-photon photopolymerization and photo-induced termination.

Proceedings SPIE 7053, Organic 3D Photonics Materials and Devices II, 70530E (3 September 2008). https://doi: 10.1117/12.796978

[165] Ahn D, Sathe SS, Clarkson BH, Scott TF. Hexaarylbiimidazoles as visible light thiol–ene photoinitiators. Dent Mater 2015;31:1075–89. https://doi.org/10.1016/j.dental.2015.06.005.

[166] Bohren CF. Absorption and scattering of light by small particles. WILEY-VCH Verlag GmbH & Co. KGaA 1983.

[167] Madrid-Wolff J, Boniface A, Loterie D, Delrot P, Moser C. Controlling Light in Scattering Materials for Volumetric Additive Manufacturing. Adv Sci 2022;9:2105144. https://doi.org/10.1002/advs.202105144.

[168] Lucía Rodríguez-Pombo, Xu X, Alejandro Seijo-Rabina, Ong JJ, Alvarez-Lorenzo C, Carlos Rial, et al. Volumetric 3D printing for rapid production of medicines. Addit Manuf 2022;52:102673. https://doi.org/10.1016/j.addma.2022.102673.

[169] Salajeghe R, Meile DH, Kruse CS, Marla D, Spangenberg J. Numerical modeling of part sedimentation during volumetric additive manufacturing. Addit Manuf 2023;66:103459. https://doi.org/10.1016/J.ADDMA.2023.103459.

[170] Karnes JJ, Weisgraber TH, Cook CC, Wang DN, Crowhurst JC, Fox CA, et al. Isolating Chemical Reaction Mechanism as a Variable with Reactive Coarse-Grained Molecular Dynamics: Step-Growth versus Chain-Growth Polymerization. Macromolecules 2023;56:2225-33. https://doi.org/10.1021/ACS.MACROMOL.2C02069.

[171] Loterie D, Delrot P, Moser C. Volumetric 3D printing of elastomers by tomographic back-projections. 2018 [Preprint] Available from: https://www.epfl.ch/labs/lapd/wp-content/uploads/2018/11/ms3790.pdf

[172] Loshaek S, Fox TG. Cross-linked Polymers. I. Factors Influencing the Efficiency of Cross-linking in Copolymers of Methyl Methacrylate and Glycol Dimethacrylates [1]. J Am Chem Soc 1953;75:3544–50. https://doi.org/10.1021/ja01110a068.

[173] Topa-Skwarczyńska M, Ortyl J. Photopolymerization shrinkage: strategies for reduction, measurement methods and future insights. Polym Chem 2023;14:2145–58. https://doi.org/10.1039/D3PY00261F.

[174] Stansbury J, Trujillolemon M, Lu H, Ding X, Lin Y, Ge J. Conversion-dependent shrinkage stress and strain in dental resins and composites. Dent Mater 2005;21:56–67. https://doi.org/10.1016/j.dental.2004.10.006.

[175] Hoyle CE, Bowman CN. Thiol-Ene Click Chemistry. Angew Chem Int Ed 2010;49:1540–73. https://doi.org/10.1002/anie.200903924.

[176] Shusteff M. Volumetric Additive Manufacturing of Polymer Structures by Holographically Projected Light Fields. PhD thesis. MASSACHUSETTS INSTITUTE OF TECHNOLOGY, 2017. Available from: https://dspace.mit.edu/bitstream/handle/1721.1/113939/1023862958-MIT.pdf

[177] Salajeghe R, Kruse CS, Meile DH, Marla D, Spangenberg J. Investigating the influence of thermal and mechanical properties of resin on the sedimentation rate of the printed geometry in the volumetric additive manufacturing technique. Proceedings 33rd Annual International Solid Freeform Fabrication Symposium 2022. https://doi.org/10.26153/TSW/44203.

[178] Toombs JT, Shan IK, Taylor HK. Ethyl Cellulose-Based Thermoreversible Organogel Photoresist for Sedimentation-Free Volumetric Additive Manufacturing. Macromol Rapid Commun 2023;44:2200872. https://doi.org/10.1002/marc.202200872.

[179] Lewis JA. Direct Ink Writing of 3D Functional Materials. Adv Funct Mater 2006;16:2193–204. https://doi.org/10.1002/adfm.200600434.

[180] Bhattacharya I, Toombs J, Taylor H. High fidelity volumetric additive manufacturing. Addit Manuf 2021;47:102299. https://doi.org/10.1016/J.ADDMA.2021.102299.

[181] Rackson CM, Champley KM, Toombs JT, Fong EJ, Bansal V, Taylor HK, et al. Object-space optimization of tomographic reconstructions for additive manufacturing. Addit Manuf 2021;48:102367. https://doi.org/10.1016/J.ADDMA.2021.102367.

[182] Rackson CM, Toombs JT, Beer MPD, Cook CC, Shusteff M, Taylor HK, et al. Latent image volumetric additive manufacturing. Opt Lett 2022;47:1279–82. https://doi.org/10.1364/OL.449220.

[183] Li CC, Toombs J, Taylor H. Tomographic color Schlieren refractive index mapping for computed axial lithography. Proceedings SCF 2020: ACM Symposium on Computational Fabrication 2020. https://doi.org/10.1145/3424630.3425421.

[184] Orth A, Sampson KL, Zhang Y, Ting K, Van Egmond DA, Laqua K, et al. On-the-fly 3D metrology of volumetric additive manufacturing. Addit Manuf 2022;56:102869. https://doi.org/10.1016/j.addma.2022.102869.

[185] Biria S, Malley PPA, Kahan TF, Hosein ID. Tunable Nonlinear Optical Pattern Formation and Microstructure in Cross-Linking Acrylate Systems during Free-Radical Polymerization.J Phys Chem C 2016;120:4517–28. https://doi.org/10.1021/acs.jpcc.5b11377.

[186] Liu H, Parth Chansoria, Delrot P, Emmanouil Angelidakis, Rizzo R, Rütsche D, et al. Filamented Light (FLight) Biofabrication of Highly Aligned Tissue-engineered Constructs. Adv Mater 2022;34:e2204301. https://doi.org/10.1002/adma.202204301.

[187] Jacobsen AJ, Barvosa-Carter W, Nutt S. Micro-scale Truss Structures formed from Self-Propagating Photopolymer Waveguides. Adv Mater 2007;19:3892–6. https://doi.org/10.1002/adma.200700797.

[188] Jacobsen AJ, Barvosa-Carter W, Nutt S. Compression behavior of micro-scale truss structures formed from self-propagating polymer waveguides. Acta Mater 2007;55:6724–33. https://doi.org/10.1016/j.actamat.2007.08.036.

[189] Schaedler TA, Jacobsen AJ, Torrents A, Sorensen AE, Lian J, Greer JR, et al. Ultralight Metallic Microlattices. Science 2011;334:962–5. https://doi.org/10.1126/science.1211649.

[190] Tran-Cong-Miyata Q, Nakanishi H. Phase separation of polymer mixtures driven by photochemical reactions: current status and perspectives: Phase separation of reacting polymer mixture. Polym Int 2017;66:213–22. https://doi.org/10.1002/pi.5243.

[191] Dong Z, Cui H, Zhang H, Wang F, Zhan X, Mayer F, et al. 3D printing of inherently nanoporous polymers via polymerization-induced phase separation. Nat Commun 2021;12:1–12. https://doi.org/10.1038/s41467-020-20498-1.

[192] Moore DG, Barbera L, Masania K, Studart AR. Three-dimensional printing of multicomponent glasses using phase-separating resins. Nat Mater 2020;19:212–7. https://doi.org/10.1038/s41563-019-0525-y.

[193] van de Hulst HC. Light scattering by small particles. Q J R Meteorol 1958;84:198-99. https://doi.org/10.1002/qj.49708436025

[194] Doualle T, André J-C, Gallais L. 3D printing of silica glass through a multiphoton polymerization process. Opt Lett 2021;46:364. https://doi.org/10.1364/ol.414848.

[195] Kotz F, Quick AS, Risch P, Martin T, Hoose T, Thiel M, et al. Two-Photon Polymerization of Nanocomposites for the Fabrication of Transparent Fused Silica Glass Microstructures. Adv Mater 2021;33:2006341. https://doi.org/10.1002/adma.202006341.

[196] Kak AC, Slaney M, Wang G. Principles of Computerized Tomographic Imaging. Classics In Applied Mathematics, Siam 1st Ed. 1987.

[197] Toombs J, Taylor HK. Design of a tomographic projection lithography process for roll-to-roll fabrication of 3D microstructures. Proceedings SPIE 11610, Novel Patterning Technologies 2021, 116100E (22 February 2021); https://doi.org/10.1117/12.2584009.

[198] Orth A, Sampson KL, Ting K, Boisvert J, Paquet C. Correcting ray distortion in tomographic additive manufacturing. Opt Express 2021;29:11037–54. https://doi.org/10.1364/oe.419795.

[199] Webber D, Zhang Y, Picard M, Boisvert J, Paquet C, Orth A. Versatile volumetric additive manufacturing with 3D ray tracing. Opt Express 2023;31:5531. https://doi.org/10.1364/OE.481318.

[200] O'Sullivan TD, Cerussi AE, Cuccia DJ, Tromberg BJ. Diffuse optical imaging using spatially and temporally modulated light. J Biomed Opt 2012;17:0713111. https://doi.org/10.1117/1.JBO.17.7.071311.

[201] Zvagelsky R, Mayer F, Beutel D, Rockstuhl C, Gomard G, Wegener M. Towards *in-situ* diagnostics of multi-photon 3D laser printing using optical coherence tomography. Light Adv Manuf 2022;3:1. https://doi.org/10.37188/lam.2022.039.

[202] He Y, Shao Q, Chen S-C, Zhou R. Characterization of two-photon photopolymerization fabrication using high-speed optical diffraction tomography. Addit Manuf 2022;60:103293. https://doi.org/10.1016/j.addma.2022.103293.

[203] Zvagelsky R, Kiefer P, Weinacker J, Wegener M. In-situ Quantitative Phase Imaging during Multi-photon Laser Printing. ACS Photonics 2023;10:2901-8. https://doi.org/10.1021/acsphotonics.3c00625.

[204] Li CC, Toombs J, Luk SM, de Beer MP, Schwartz JJ, Shusteff M, et al. Computational optimization and the role of optical metrology in tomographic additive manufacturing. Proceedings SPIE 12012, Advanced Fabrication Technologies for Micro/Nano Optics and Photonics XV, 1201207 (5 March 2022); https://doi.org/10.1117/12.2610558.

[205] Schwartz J, Terrel-Perez D. Optical Imaging Methods for Volumetric Additive Manufacturing. Academic J Polym Sci 2023;6:555679. https://doi.org/10.19080/AJOP.2023.06.555679.

[206] Ahn D, Stevens LM, Zhou K, Page ZA. Rapid High-Resolution Visible Light 3D Printing. ACS Cent Sci 2020;6:1555–63. https://doi.org/10.1021/acscentsci.0c00929.

[207] Stevens LM, Tagnon C, Page ZA. "Invisible" Digital Light Processing 3D Printing with Near Infrared Light. ACS Appl Mater Interfaces 2022;14:22912–20. https://doi.org/10.1021/acsami.1c22046.

[208] Stevens LM, Recker EA, Zhou KA, Garcia VG, Mason KS, Tagnon C, et al. Counting All Photons: Efficient Optimization of Visible Light 3D Printing. Adv Mater Technol 2023:2300052. https://doi.org/10.1002/admt.202300052.

[209] Mukherjee S, Schwartz J, Chang T, Baluyot E, Tringe J, Shusteff M. Focused microwave radiation for the localized curing of polymer resins. Proceedings IEEE 2022, International Symposium on Antennas and Propagation and USNC-URSI Radio Science Meeting, AP-S/URSI 2022:159–60. https://doi.org/10.1109/AP-S/USNC-URSI47032.2022.9886029.

[210] Yu Z, Li H, Zhong T, Park J-H, Cheng S, Woo CM, et al. Wavefront shaping: A versatile tool to conquer multiple scattering in multidisciplinary fields. Innovation 2022;3:100292. https://doi.org/10.1016/j.xinn.2022.100292.

[211] Habibi M, Foroughi S, Karamzadeh V, Packirisamy M. Direct sound printing. Nat Commun 2022;13:1–11. https://doi.org/10.1038/s41467-022-29395-1.

[212] Melde K, Kremer H, Shi M, Seneca S, Frey C, Platzman I, et al. Compact holographic sound fields enable rapid one-step assembly of matter in 3D. Sci Adv 2023;9:eadf6182. https://doi.org/ 10.1126/sciadv.adf6182

[213] Pingali R, Saha SK. Reaction-Diffusion Modeling of Photopolymerization during Femtosecond Projection Two-Photon Lithography. J Manuf Sci Eng 2021;144:1–13. https://doi.org/10.1115/1.4051830.

[214] Arnoux C, Pérez-Covarrubias LA, Khaldi A, Carlier Q, Baldeck PL, Heggarty K, et al. Understanding and overcoming proximity effects in multi-spot two-photon direct laser writing. Addit Manuf 2022;49:102491. https://doi.org/10.1016/j.addma.2021.102491.

[215] Johnson JE, Chen Y, Xu X. Model for polymerization and self-deactivation in two-photon nanolithography. Opt Express 2022;30:26824. https://doi.org/10.1364/OE.461969.

[216] Somers P, Liang Z, Chi T, Johnson JE, Pan L, Boudouris BW, et al. Photo-activated polymerization inhibition process in photoinitiator systems for high-throughput 3D nanoprinting. Nanophotonics 2023;12:1571–80. https://doi.org/10.1515/nanoph-2022-0611.

[217] Karnes JJ, Weisgraber TH, Oakdale JS, Mettry M, Shusteff M, Biener J. On the Network Topology of Cross-Linked Acrylate Photopolymers: A Molecular Dynamics Case Study. J Phys Chem B 2020;124:9204–15. https://doi.org/10.1021/acs.jpcb.0c05319.

[218] Loutfy RO. High-conversion polymerization of fluorescence probes. 1. Polymerization of methyl methacrylate. Macromolecules 1981;14:270–5. https://doi.org/10.1021/ma50003a009.

[219] Bosch P, Fernández-Arizpe A, Mateo JL, Catalina F, Peinado C. New fluorescent probes for monitoring the polymerization reaction: p-vinyliden derivatives of N,N-dimethylaminoaryl compounds. J Photochem Photobiol A: Chem 2002;153:135–43. https://doi.org/10.1016/S1010-6030(02)00260-5.

[220] Ma C, Sun W, Xu L, Qian Y, Dai J, Zhong G, et al. A minireview of viscosity-sensitive fluorescent probes: design and biological applications. J Mater Chem B 2020;8:9642–51. https://doi.org/10.1039/D0TB01146K.

[221] Yang X, Zhang D, Ye Y, Zhao Y. Recent advances in multifunctional fluorescent probes for viscosity and analytes. Coord Chem Rev 2022;453:214336. https://doi.org/10.1016/j.ccr.2021.214336.

[222] Liu J, Liu Y, Bu W, Bu J, Sun Y, Du J, et al. Ultrasensitive Nanosensors Based on Upconversion Nanoparticles for Selective Hypoxia Imaging in Vivo upon Near-Infrared Excitation. J Am Chem Soc 2014;136:9701–9. https://doi.org/10.1021/ja5042989.

[223] Wang X, Wolfbeis OS. Optical methods for sensing and imaging oxygen: materials, spectroscopies and applications. Chem Soc Rev 2014;43:3666–761. https://doi.org/10.1039/C4CS00039K.

[224] Rizzo R, Petelinšek N, Bonato A, Zenobi-Wong M. From Free-Radical to Radical-Free: A Paradigm Shift in Light-Mediated Biofabrication. Adv Sci 2023;10:2205302. https://doi.org/10.1002/advs.202205302.

[225] Breugst M, Reissig H-U. The Huisgen Reaction: Milestones of the 1,3-Dipolar Cycloaddition. Angew Chem Int Ed 2020;59:12293–307. https://doi.org/10.1002/anie.202003115.

[226] Briou B, Améduri B, Boutevin B. Trends in the Diels–Alder reaction in polymer chemistry. Chem Soc Rev 2021;50:11055–97. https://doi.org/10.1039/D0CS01382J.

[227] Zhu G, Hou Y, Xu J, Zhao N. Reprintable Polymers for Digital Light Processing 3D Printing. Adv Funct Mater 2021;31:2007173. https://doi.org/10.1002/adfm.202007173.

[228] Li H, Zhang B, Wang R, Yang X, He X, Ye H, et al. Solvent-Free Upcycling Vitrimers through Digital Light Processing-Based 3D Printing and Bond Exchange Reaction. Adv Funct Mater 2022;32:2111030. https://doi.org/10.1002/adfm.202111030.

[229] Shi Q, Yu K, Kuang X, Mu X, Dunn CK, Dunn ML, et al. Recyclable 3D printing of vitrimer epoxy. Mater Horiz 2017;4:598–607.https://doi.org/10.1039/C7MH00043J.

[230] Lu P, Pengtao Lu, Ahn D, Yunis R, Delafresnaye L, Corrigan N, et al. Wavelength-selective light-matter interactions in polymer science. Matter 2021;4:2172–229. https://doi.org/10.1016/j.matt.2021.03.021.

[231] Jan Hobich, Eva Blasco, Martin Wegener, Hatice Mutlu, Barner-Kowollik C. Synergistic, Orthogonal, and Antagonistic Photochemistry for Light-Induced 3D Printing. Macromol Chem Phys 2022;224:2200318. https://doi.org/10.1002/macp.202200318.

[232] Blasco E, Müller J, Müller P, Trouillet V, Schön M, Scherer T, et al. Fabrication of Conductive 3D Gold-Containing Microstructures via Direct Laser Writing. Adv Mater 2016;28:3592–5. https://doi.org/10.1002/adma.201506126.

[233] Tabrizi S, Cao Y, Cumming BP, Jia B, Gu M.Functional Optical Plasmonic Resonators Fabricated via Highly Photosensitive Direct Laser Reduction. Adv Opt Mater 2016;4:529–33.https://doi.org/10.1002/adom.201500568.

[234] Ma Z-C, Zhang Y-L, Han B, Chen Q-D, Sun H-B. Femtosecond-Laser Direct Writing of Metallic Micro/Nanostructures: From Fabrication Strategies to Future Applications. Small Methods 2018;2:1700413. https://doi.org/10.1002/smtd.201700413.

[235] Luitz M, Pellegrini D, Von Holst M, Seteiz K, Gröner L, Schleyer M, et al. High-Resolution Patterning of Organic–Inorganic Photoresins for Tungsten and Tungsten

Carbide Microstructures. Adv Eng Mater 2023;25:2201927. https://doi.org/10.1002/adem.202201927.

[236] Saccone MA, Gallivan RA, Narita K, Yee DW, Greer JR. Additive manufacturing of micro-architected metals via hydrogel infusion. Nature 2022;612:685–90. https://doi.org/10.1038/s41586-022-05433-2.

Graphical abstract

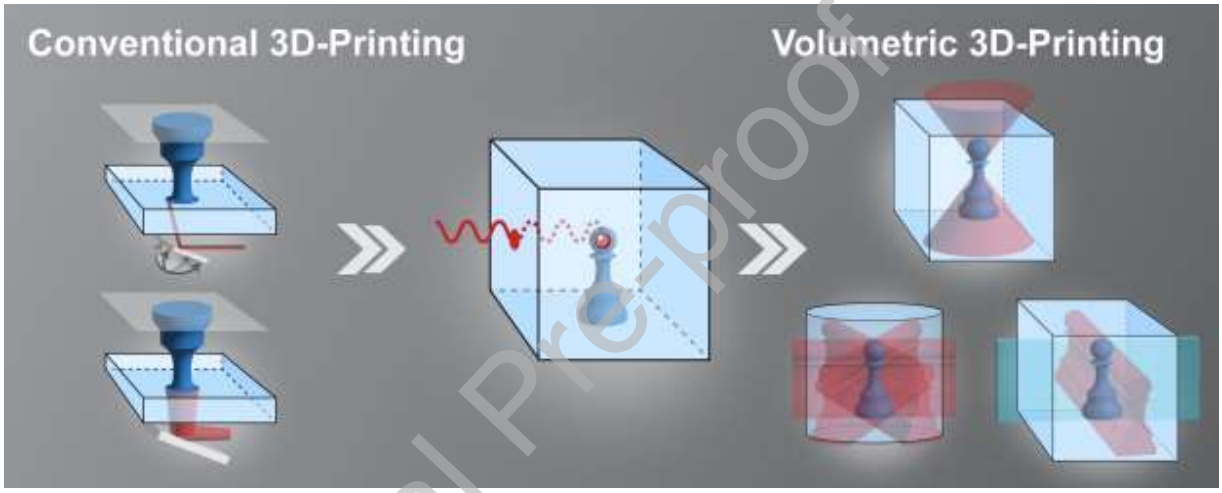

Declaration of interests

☐ The authors declare that they have no known competing financial interests or personal relationships that could have appeared to influence the work reported in this paper.

☒The authors declare the following financial interests/personal relationships which may be considered as potential competing interests:

HKT is an inventor on U.S. patents 10,647,061 11,370,173, and 11,639,031, which describe the CAL process.